BIOCHEMISTRY
including biophysical chemistry & molecular biology

Article

pubs.acs.org/biochemistry

# Mutant IDH1 Enhances the Production of 2-Hydroxyglutarate Due to Its Kinetic Mechanism

Alan R. Rendina, Beth Pietrak, Angela Smallwood, Huizhen Zhao, Hongwei Qi, Chad Quinn, Nicholas D. Adams, Nestor Concha, Chaya Duraiswami, Sara H. Thrall, Sharon Sweitzer, and Benjamin Schwartz*

Departments of Biological Reagents and Assay Development, Cancer Epigenetics, and Computational and Structural Chemistry, GlaxoSmithKline, 1250 South Collegeville Road, Collegeville, Pennsylvania 19426, United States

Supporting Information

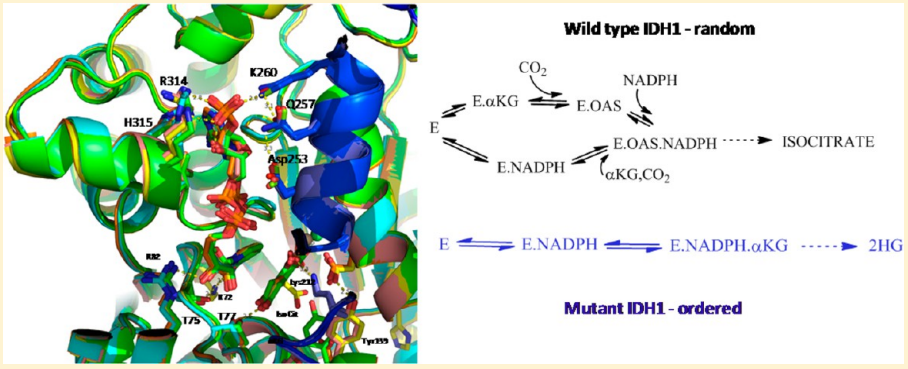


**ABSTRACT:** The human, cytosolic enzyme isocitrate dehydrogenase 1 (IDH1) reversibly converts isocitrate to α-ketoglutarate (αKG). Cancer-associated somatic mutations in IDH1 result in a loss of this normal function but a gain in a new or neomorphic ability to convert αKG to the oncometabolite 2-hydroxyglutarate (2HG). To improve our understanding of the basis for this phenomenon, we have conducted a detailed kinetic study of wild-type IDH1 as well as the known 2HG-producing clinical R132H and G97D mutants and mechanistic Y139D and (newly described) G97N mutants. In the reductive direction of the normal reaction (αKG to isocitrate), dead-end inhibition studies suggest that wild-type IDH1 goes through a random sequential mechanism, similar to previous reports on related mammalian IDH enzymes. However, analogous experiments studying the reductive neomorphic reaction (αKG to 2HG) with the mutant forms of IDH1 are more consistent with an ordered sequential mechanism, with NADPH binding before αKG. This result was further confirmed by primary kinetic isotope effects for which saturating with αKG greatly reduced the observed isotope effect on $^{D}(V/K)_{NADPH}$. For the mutant IDH1 enzyme, the change in mechanism was consistently associated with reduced efficiencies in the use of αKG as a substrate and enhanced efficiencies using NADPH as a substrate. We propose that the sum of these kinetic changes allows the mutant IDH1 enzymes to reductively trap αKG directly into 2HG, rather than allowing it to react with carbon dioxide and form isocitrate, as occurs in the wild-type enzyme.

An unbiased analysis of glioblastoma exomes first identified frequent somatic mutations in the metabolic enzyme isocitrate dehydrogenase 1 (IDH1).[1] In the past several years, mutations in IDH1, and the related isoform IDH2, have been found in several different types of cancers, including AML,[2−4] ALL,[5] MDS,[6] chondrosarcomas,[7] AITL,[8] cholangiocarcinomas,[9] and pancreatic cancer.[10] Mutations were found to occur at specific amino acids along the protein sequence and to be heterozygously expressed, consistent with a gain of function. However, these mutations occur at functionally conserved residues,[11,12] and biochemical studies of the mutant forms of IDH1 demonstrated a loss of the normal function of IDH1, the reversible conversion of isocitrate to α-ketoglutarate (αKG).[13,14] However, using a metabolomic approach, it was subsequently shown that the result of these mutations is to allow a new (or neomorphic) conversion of αKG to 2-hydroxyglutarate (2HG).[15] As a result, cancers that harbor mutant forms of IDH1 display increases in 2HG concentrations of nearly 100-fold.[4,15]

The role of 2HG as an oncometabolite has been linked to its ability to compete with αKG for binding to mononuclear, non-heme iron dioxygenases that utilize αKG as a redox cofactor. These enzymes include epigenetic regulators such as the Jumonji family of histone demethylases[16] and Tet2,[17] which hydroxylates 5-methylcytosine as a purported initiating step in DNA demethylation. As a result of this inhibition, cells with

Received: April 24, 2013
Revised: May 24, 2013
Published: June 3, 2013

  

IDH1 or IDH2 mutations display hypermethylation of histones and DNA and related alterations in transcription.[18,19]

While the correlation between IDH1 and IDH2 mutations and enhanced 2HG production is well established, a rationale for the causation is still developing. To address this gap, we have investigated the structures and kinetics for the wild-type and several IDH1 mutants, including a newly described mechanistic G97N form of the enzyme. While we did not observe any recurring themes from these structures that we could associate with the ability of an IDH1 enzyme to make 2HG, we did note consistent changes in mutant IDH1 enzyme kinetics.

In steady state measurements of the reductive chemical reactions, all of the 2HG-producing mutants of IDH1 displayed a reduced catalytic efficiency with the substrate αKG and an increased efficiency with NADPH relative to that of the wild-type enzyme. Further, in conjunction with the changes in substrate utilization, we found that while the wild-type enzyme displays a random sequential kinetic mechanism, all of the mutant enzymes prefer an ordered sequential mechanism, determined using a combination of dead-end inhibition patterns and primary isotope effect methods. The combination of these results offers an explanation for the kinetic changes in mutant forms of IDH1 that drive the increased level of 2HG production.

## MATERIALS AND METHODS

$NADP^+$, NADPH, *N*-oxalylglycine, $NAADP^+$, $d_8$-2-propanol, *Thermoanaerobacter brockii* alcohol dehydrogenase, diaphorase, resazurin, resorufin, 6-methoxy-2-naphthaldehyde, and aldehyde dehydrogenase were purchased from Sigma-Aldrich. αKG was purchased from Fluka. Racemic isocitrate was purchased from MP Biomedicals, LLC. 2HG was purchased from Toronto Research Chemicals. Pro-*R*-NADPH and NADPD were prepared from $NADP^+$ and $d_8$-2-propanol with *T. brockii* alcohol dehydrogenase as described by Pollock and Barber.[20]

**Preparation of 2-Hydroxyglutarate-$d_4$ ($d_4$-2HG).** A solution of α-ketoglutarate-$d_6$ (500 mg, 3.33 mmol) in water (5 mL) was treated dropwise with a solution of sodium borohydride (87 mg, 2.291 mmol) in water (5.00 mL) and stirred for 5 min. The mixture was treated with 1 M hydrochloric acid (0.32 mL) and then freeze-dried overnight to give the crude product as an off-white solid. The solid was purified by preparative high-performance liquid chromatography (HPLC) (ZIC-HILIC column, EMD, 5 μm, 200 Å, 4.6 mm × 150 mm; 80:20:0.01 $CH_3CN/H_2O/NH_4OH$; 20 mL/min; UV 205 nm) to provide 2-hydroxyglutarate-$d_4$ (131 mg, 0.844 mmol, 25.3% yield) as a tan solid.

**Production of Homodimeric Wild-Type, R132H, G97D, G97N, and Y139D IDH1.** The open reading frame of IDH1 was amplified from human brain cDNA (NM_005896) and cloned into the pENTR/TEV/D-TOPO vector (Life Technologies). In-Fusion (Clontech Laboratories, Inc.) was used to insert IDH1 into the *Escherichia coli* expression vector pET41a with a C-terminal $His_8$ tag. R132H, G97D, G97N, and Y139D IDH1 mutations were introduced using a QuikChange site-directed mutagenesis kit (Agilent Technologies). Wild-type and mutant proteins were expressed in the Rosetta 2(DE3) strain (EMD Millipore).[15] For specific enzyme activity measurements, small-scale proteins were purified with MagneHis Ni-Particles (Promega). For detailed kinetic experiments, proteins were first purified on a Ni-NTA SuperFlow resin (Qiagen) followed by a size exclusion Superdex 200 column (GE). In addition to kinetic determinations, the resulting purified proteins were concentrated to 15−20 mg/mL and used for crystallography and generation of cofactor-free reagents.

**Generation of Cofactor-Free IDH1.** Ten milligrams of purified IDH1 was bound to 1 mL of NiNTA beads by being mixed at room temperature for 1 h. In a 10 mL disposable dripping column, the beads were washed at room temperature first with 20 mL of protein storage buffer [50 mM Tris (pH 7.5) and 100 mM NaCl], followed by 50 mL of substrate buffer containing 10 mM $MgCl_2$ and 20 mM αKG for mutant proteins or 10 mM $MgCl_2$, 20 mM αKG, and 100 mM bicarbonate for wild-type (WT) IDH1 to convert NADPH to $NADP^+$. Lastly, the beads were again washed with 50 mL of the protein storage buffer to remove the less tightly bound $NADP^+$. Proteins were eluted from the Ni beads with storage buffer containing 200 mM imidazole, and the protein solution was exchanged with protein storage buffer using a Zaba desalting column (Pierce). The final products were concentrated to >5 mg/mL and assayed for cofactor stoichiometry as well as enzyme activity. All samples were found to retain full enzymatic activity after treatment.

The levels of bound $NADP^+$ and NADPH before and after treatment were obtained by heat denaturing the IDH1 protein (incubation for 5 min at 85 °C followed by snap incubation on ice for 5 min), and then detection of the unbound cofactor via a coupled enzyme assay. For $NADP^+$ quantitation, aldehyde dehydrogenase was used to convert free $NADP^+$ to NADPH with the concomitant oxidation of 6-methoxy-2-naphthaldehyde to the fluorogenic product 6-methoxy-2-naphthoate (excitation at 310 nm and emission at 375 nm). Assays were conducted in a 20 μL volume in a 384-well microplate (Greiner 784076) in buffer consisting of 100 mM Tris (pH 8.0), 10 mM $MgCl_2$, 0.05% CHAPS, 0.01% BSA, 100 μM 6-methoxy-2-naphthaldehyde, and 6.25 mg/mL aldehyde dehydrogenase, with concentrations of IDH1 varying from 10 to 50 μM. For NADPH quantitation, diaphorase was used to catalyze the NADPH-dependent reduction of resazurin to the fluorescent product resorufin (excitation at 530 nm and emission at 580 nm). Assays were conducted in a 10 μL volume in a 384-well microplate (Greiner 784076) in buffer consisting of 100 mM Tris (pH 8.0), 10 mM $MgCl_2$, 0.05% CHAPS, 0.01% BSA, 12.5 μM resazurin, and 1.25 units/mL diaphorase, with concentrations of IDH1 varying from 10 to 50 μM. Standard curves of the fluorescent products were used to quantitate $NADP^+$ and NADPH.

**Crystallization, Structure Determination, and Refinement of Closed Wild-Type and Mutant IDH1 Structures.** Homodimers of human R132H, G97D, Y139D, and G97N IDH1 were crystallized in the presence of ligands following the same procedure. The enzyme (14 mg/mL) was incubated on ice for 1 h with 10 mM NADPH (MP Biomedicals catalog no. 0215174225), 20 mM $CaCl_2$, and 75 mM αKG (pH 7). The crystals were grown at 20 °C by sitting drop vapor diffusion in drops containing 2 μL of the IDH1 complex and 2 μL of a reservoir solution containing PEG 3350 (12−22%), 100 mM Bis-Tris (pH 7), and 200 mM calcium acetate. The crystals appeared overnight and grew to full size in 5 days. Prior to data collection, 20 μL of a cryogenic solution [20% ethylene glycol, 24% PEG 3350, 100 mM Bis-Tris (pH 7.0), and 200 mM calcium acetate] was added slowly to the crystallization drop, and the crystals were flash-frozen in liquid $N_2$. For the wild-type enzyme, a 20 mg/mL protein sample was incubated on ice for 1 h with $NADP^+$, 10 mM $CaCl_2$, and 10 mM isocitrate (pH 7).


dx.doi.org/10.1021/bi400514k | *Biochemistry* 2013, 52, 4563−4577

The crystals were grown at 20 °C by sitting drop vapor diffusion in drops containing 2 μL of the IDH1 complex and 2 μL of a reservoir solution containing a range of PEG MME 2000 concentrations (16−20%) and 100 mM 2-(*N*-morpholino)ethanesulfonic acid (MES) (pH 6.9). The crystals appeared overnight and grew to full size in 5 days. Prior to data collection, 20 μL of a cryogenic solution [20% ethylene glycol, 22% PEG MME 2000, and 100 mM MES (pH 6.9)] was added slowly to the crystallization drop and the crystals were flash-frozen in liquid $N_2$.

The diffraction data were collected at Argonne National Laboratory, Advanced Photon Source, Sector 21, and the diffraction data were processed with HKL2000.[21] The structures were determined by molecular replacement using Phaser[22] as implemented in the CCP4 suite[23] and refined using Refmac5. The *R* factor was monitored using a randomly selected 5% of the reflections and set aside for calculation of $R_{free}$.[24] The stereochemistry and overall quality of the models were evaluated using Molprobity,[25] and the necessary adjustments were made using COOT.[26] Crystallization statistics are listed in Table 1 of the Supporting Information.

***In Silico* Multifragment Search (MFS).** This method, as implemented in the Molecular Operating Environment (MOE)[27] from the Chemical Computing group (CCG), is similar to the MCSS method developed at Harvard by the Karplus group.[28] For this MFS analysis, the MMFF94X potential function along with a distance-dependent dielectric function was used to compute the electrostatistics and solvation energy terms. In this method, a protein active site is flooded with a large number of randomly placed molecular fragments. A special energy minimization protocol is then used to refine fragment positions and orientations, where the receptor atoms feel the average forces of the fragments, while each fragment feels the full force of the receptor but not of the other fragments, and fragment overlap is neglected. In the case of IDH1, our goal was to identify areas in the enzyme where $CO_2$ molecules are predicted to be more energetically favorable, in an attempt to understand how these $CO_2$ molecules might access the active site pocket. For this analysis, a box 12 Å in diameter surrounding the isocitrate binding site of WT IDH1 was flooded with $CO_2$ molecules. The enzyme was constrained to the crystal structure coordinates during the minimization process to assess where $CO_2$ molecules would want to cluster in a known low-energy conformation of the protein. Duplicate $CO_2$ molecules within a specified root-mean-square (rms) deviation tolerance (0.2 Å) in each $CO_2$ cluster were deleted and the unique $CO_2$ molecules along with the calculated interaction energies were mapped onto the WT structure for further analysis.

**Measurement of IDH1-Mediated Conversion of Isocitrate to αKG.** The conversion of isocitrate to αKG was monitored by coupling the second reaction product NADPH to diaphorase, which catalyzes a NADPH-dependent reduction of resazurin to the fluorescent product resorufin (excitation at 530 nm and emission at 580 nm). Assays were conducted in a 10 μL volume in a 384-well microplate (Greiner 784076) in a buffer consisting of 100 mM Tris (pH 8.0), 10 mM $MgCl_2$, 0.05% CHAPS, 0.01% BSA, 12.5 μM resazurin, 1.25 units/mL diaphorase, and 0.5 nM WT IDH1, with varying concentrations of either isocitrate or $NADP^+$. When the concentration of isocitrate was varied, the level of $NADP^+$ was held at fixed, saturating concentrations (typically 50 μM). When the concentration of $NADP^+$ was varied, the level of isocitrate was held at fixed, saturating concentrations (typically 100 μM). For IDH1 mutants with lower $k_{cat}$ values, higher enzyme concentrations were used.

**Measurement of the αKG to Isocitrate Reaction (WT IDH1) by Absorbance Spectroscopy.** The inhibition mechanisms for inhibitors of WT IDH1 were determined by monitoring the oxidation of NADPH by the decrease in absorbance at 340 nm in the presence of αKG and sodium bicarbonate, in which the concentration of one of these substrates was varied and the other substrates were fixed at either saturating or subsaturating concentrations in the presence of varied inhibitor concentrations. Reactions were conducted at 25 °C in 96-well 1/2 area microtiter plates (Corning 3884) in a final volume of 100 μL in assay buffer consisting of 100 mM Tris (pH 8.0), 10 mM $MgCl_2$, 0.05% CHAPS, 0.01% BSA, and 0.1 mM DTT with 2.5−5 nM human full-length WT IDH1, and variable concentrations of NADPH (typically from 25 to 400 μM from a 10 mM stock calibrated using an extinction coefficient of 6.22 $mM^{-1}$ $cm^{-1}$ at 340 nm), αKG (typically 0.125 to 4 mM from a 250 mM stock), sodium bicarbonate (typically from 6.25 to 100 mM from a 1 M stock), N-OG (typically from 0.2 to 12.8 mM from a 170 mM stock), and $NAADP^+$ (typically from 0.0625 to 4 mM from a 10 mM stock). Controls were conducted in the absence of WT IDH1 to correct for nonenzymatic oxidation of NADPH. Absorbance changes were monitored continuously using an EnVision Multilabel Reader (PerkinElmer). This method was also used to measure the primary isotope effects for WT and mutant IDH1 at fixed high NADPH(D) concentrations and fixed concentrations of αKG and $CO_2$ (sodium bicarbonate; WT only) as indicated in the tables. Concentrations of NADPH and NADPD were calibrated on the day of use as described above.

**Liquid Chromatography−Tandem Mass Spectrometry (LC−MS/MS) Methods for Isocitrate and 2HG Detection.** All analyses were performed on an API 4000 triple-quadrupole tandem mass spectrometer (Applied Biosystems). Other instrumentation consisted of a Shimadzu binary LC10ADvp HPLC system and a HTS Pal (Leap Technologies) autosampler. LC was performed on a Phenomenex Luna C18 analytical column [150 mm × 4.6 mm (inside diameter); 5 μm particle size] with a water (solution A) and acetonitrile (solution B) gradient containing 1% acetic acid as the mobile phase. Solution A at 95% was held for 1 min, before a linear gradient from 5.0 to 90% B over 1.75 min with a hold for 1.25 min was generated by Shimadzu LC 10ADvp pumps. The 1.0 mL/min flow was directed into the mass spectrometer, which operated in the negative multiple-reaction monitoring mode. The MS/MS system was optimized by continuous infusion of each standard (10 mM) at a flow rate of 200 μL/min. 2HG was monitored by the transition from *m*/*z* 147.1 to 129.0 using a DP of −35.0, a collision energy of −16.0, and a CXP of −9.0. Isocitrate was monitored by the transition from *m*/*z* 191.0 to 173.0 using a DP of −33.0, a collision energy of −14.0, and a CXP of −7.0. The internal standard $d_4$-2HG was monitored by the transition from *m*/*z* 151.0 to 131.9 using a DP of −35.0, a collision energy of −16.0, and a CXP of −9.0. The source parameters were set as follows: temperature of the electrospray, 600 °C; collision-activated dissociation gas (nitrogen), 4; curtain gas (nitrogen) flow, 30; turbo ion gas (zero air), 50; desolvation gas (zero air), 50; ion spray voltage, 4200 V. Data were acquired and processed with Analyst for Windows (version 1.4.2). The 2HG protocol was adjusted by *m*/*z* 1 to analyze deuterated 2HG ($d_1$-2HG) product formation. The


dx.doi.org/10.1021/bi400514k | *Biochemistry* 2013, 52, 4563−4577

peak areas for 2HG, $d_1$-2HG, and isocitrate were normalized using the peak area of the internal standard $d_4$-2HG.

**RapidFire MS/MS Method for 2HG Detection.** Analyses utilized an API 4000 triple-quadrupole mass spectrometer (Applied Biosystems, Foster City, CA) coupled to a RapidFire 300 high-throughput mass spectrometry (HTMS) system (Agilent, Wakefield, MA). RapidFire SPE was conducted with a HILIC cartridge as the solid support, and liquid handling was accomplished using the RapidFire autosampler equipped with three isocratic HPLC 1100 pumps (Agilent). Samples were aspirated for approximately 150 ms from each well of a 384-well microtiter plate, of which 10 μL was then transferred to the solid-phase extraction cartridge using pump 1 at a rate of 1.5 mL/min (90:10 acetonitrile/water mixture). Following a 1000 ms (90:10 acetonitrile/water mixture) wash to remove unwanted reaction components, the analyte of interest was reverse eluted off the cartridge in 3000 ms using pump 3 at a rate of 1.25 mL/min (20:80 acetonitrile/water mixture) and introduced into the mass spectrometer source. The HILIC cartridge was then re-equilbrated using pump 1 for 3000 ms prior to the next injection. The total injection to injection cycle time was 7150 ms. The 1.25 mL/min flow was directed into the mass spectrometer, which operated in the negative multiple-reaction monitoring mode. The MS/MS system was optimized by the continuous infusion of each standard (10 mM) at a flow rate of 200 μL/min. 2HG was monitored by the transition from $m/z$ 146.9 to 128.9 using a DP of −35.0, a collision energy of −16.0, and a CXP of −5.0. The internal standard $d_4$-2HG was monitored by the transition from $m/z$ 151.0 to 131.9 using a DP of −35.0, a collision energy of −16.0, and a CXP of −5.0. The parameters were set as follows: temperature of the electrospray, 600 °C; collision-activated dissociation gas (nitrogen), 4; curtain gas (nitrogen) flow, 50; turbo ion gas (zero air), 50; desolvation gas (zero air), 50; ion spray voltage, 4200 V. Data were acquired using Analyst for Windows (version 1.4.2) and processed using Agilent's RapidFire Integrator software to integrate mass spectrometric data.

**Steady State and Dead-End Inhibition Studies.** IDH1 mutant kinetics and inhibition mechanisms with NADPH as the varied substrate were determined by measuring the formation of 2HG with the HTMS system. Reactions were conducted at room temperature in 384-well Greiner polypropylene microtiter plates in a total volume of 30 μL of assay buffer. Final (before quench) NADPH concentrations were typically varied from 0.1 to 25.6 μM; the N-OG concentration was varied from 50 to 400 μM, and the αKG concentration was typically fixed at 0.2−1 mM, depending on the mutant. Reactions were conducted in duplicate and initiated by addition of mutant enzymes [5 nM R132H, 50 nM G97D and G97N, or 100 nM Y139D (final concentrations)]. Six time points were obtained from 0 to 10 min in 2 min intervals by quenching with 200 mM EDTA (final concentration of 50 mM). At time zero, a time point was obtained by prequenching those wells with EDTA. After each addition, plates were centrifuged for 10 s to ensure complete mixing of reagents. For the HTMS analysis, a 0.5 μL aliquot of each well was diluted 200-fold into a separate analysis plate containing 200 μL of a freshly prepared methanol/acetonitrile mixture (1:1) with 0.075 μg/mL (~0.49 μM) $d_4$-2HG as an internal standard.

To determine isotope effects at low NADPH(D) concentrations (typically from 0.1 to 12.8 μM in 2-fold increments from freshly calibrated stocks), reactions were conducted as described above and analyzed using the LC−MS/MS method. These reactions were quenched with final concentrations of 100 mM EDTA and 0.33 μM $d_4$-2HG, and samples were directly injected into the LC−MS/MS system without additional dilution.

Values for the kinetic parameters and their standard errors were obtained by fitting data to the appropriate equations using the nonlinear regression function of GraFit (Erithacus Software). The initial rate data for $V_{max}$, $K_m$, and $K_{ia}$ determinations were fit to eqs 1 and 2. Data from the mechanism of inhibition studies were fit to eqs 3−6 and for the isotope effect analysis to eqs 7−9. Except where noted, the best model was determined from the lowest $\chi^2$ and lowest standard errors in the fitted parameters.

Michaelis−Menten

$$v = \frac{V_{max}[S]}{K_m + [S]} \quad (1)$$

Two-substrate sequential mechanism

$$v = \frac{(V_{max}[A][B])}{(K_{ia}K_b + K_b[A] + K_a[B] + [A][B])} \quad (2)$$

Competitive inhibition

$$v = \frac{V_{max}[S]}{K_m\left(1 + \frac{[I]}{K_i}\right) + [S]} \quad (3)$$

Noncompetitive inhibition with separate $K_i$ values

$$v = \frac{(V_{max}[S])}{\left[K_m\left(1 + \frac{[I]}{K_{is}}\right) + \left(1 + \frac{[I]}{K_{ii}}\right)[S]\right]} \quad (4)$$

Noncompetitive inhibition where $K_{is} = K_{ii}$

$$v = \frac{V_{max}[S]}{(K_m + [S])\left(1 + \frac{[I]}{K_i}\right)} \quad (5)$$

Uncompetitive inhibition

$$v = \frac{V_{max}[S]}{K_m + [S]\left(1 + \frac{[I]}{K_i}\right)} \quad (6)$$

Isotope effects on $V_{max}$ and $V/K$

$$v = \frac{(V_{max}[S])}{[K_m(1 + F_iE_{V/K}) + (1 + F_iE_V)[S]]} \quad (7)$$

Equal isotope effects on $V_{max}$ and $V/K$

$$v = \frac{(V_{max}[S])}{[K_m(1 + F_iE_V) + (1 + F_iE_V)[S]]} \quad (8)$$

Isotope effect on $V_{max}$ only

$$v = \frac{(V_{max}[S])}{[K_m + (1 + F_iE_V)[S]]} \quad (9)$$

In eqs 1−9, $v$ is the initial velocity, $V_{max}$ is the maximal velocity, [S], [A], and [B] are the varied substrate concentrations, [I] is the inhibitor concentration, $K_a$, $K_b$, and $K_m$ are Michaelis constants, $K_{ia}$ is the dissociation constant for which $\alpha = K_{ia}/K_a$, and $K_i$, $K_{is}$, and $K_{ii}$ are inhibition constants ($K_{is}$ is the dissociation constant for the E−I complex, and $K_{ii}$ is the dissociation constant for dissociation of I from the E−S−I


dx.doi.org/10.1021/bi400514k | Biochemistry 2013, 52, 4563−4577

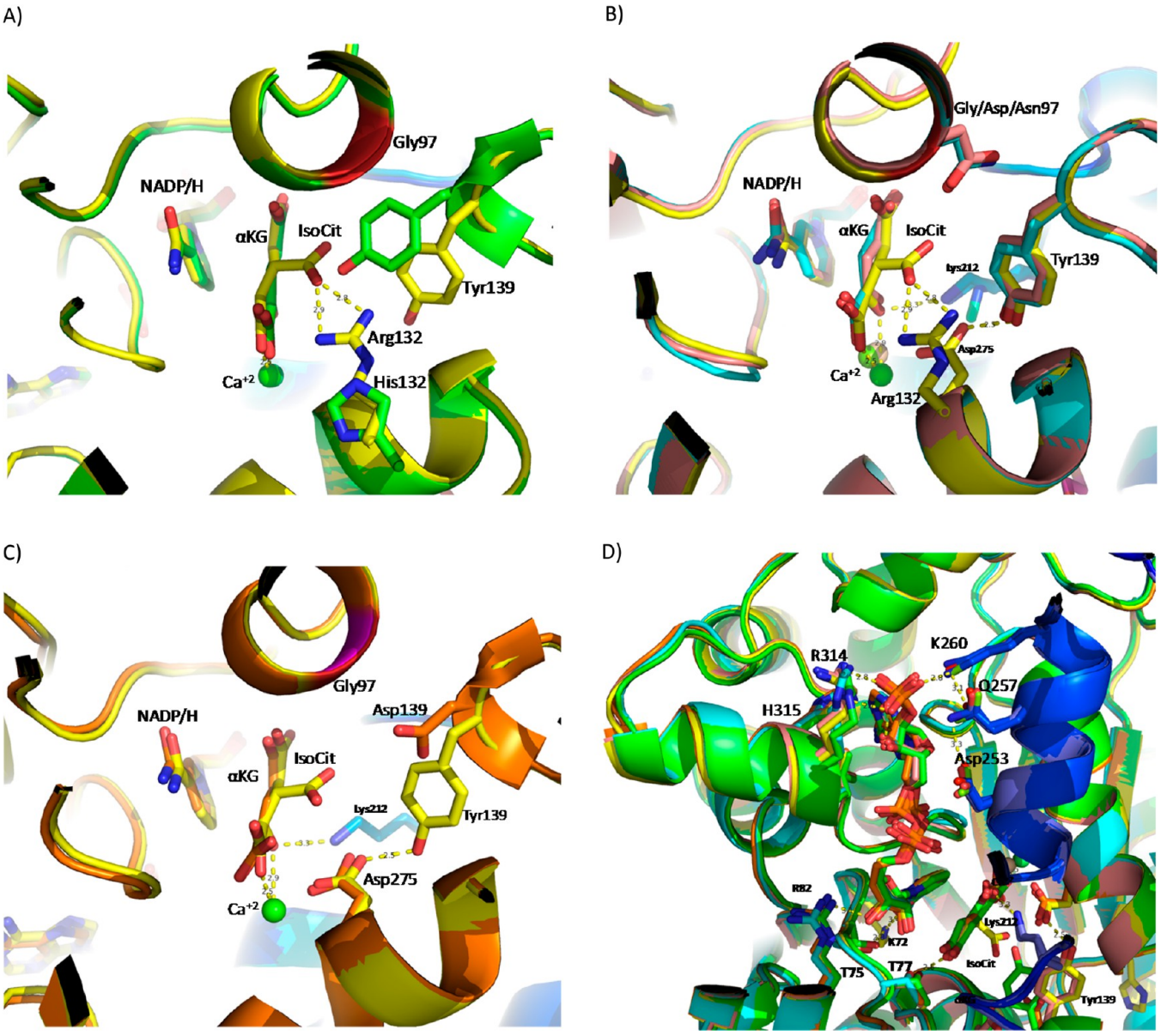


**Figure 1.** Structures of the wild-type and mutant homodimeric IDH1 enzymes with substrates bound. (A–C) Overlay of the wild-type and mutant IDH1 structures focused on the substrate binding site. (A) Structure of the wild-type (yellow) and R132H (green) demonstrating the rotation of Y139 toward the substrate binding site in the mutant enzyme. This rotation is absent in the other neomorphic mutants as demonstrated in panel B, which shows the overlay of the wild-type (yellow) with G97N (cyan) and G97D (salmon). (C) Overlay of the wild-type (yellow) and Y139D (orange). (D) Overlay of all five structures focused on the NADP/H cofactor site. For the wild-type structure, one subunit of the dimer is colored green and the other blue. No changes in the positions of the key interacting residues described in the text were observed.

complex when S is saturating). In eqs 7–9, $F_i$ is the fraction of isotopic label (0 for NADPH and 0.998 for NADPD) and $E_{V/K}$ and $E_V$ are the isotope effects minus 1 on $V_{max}/K_m$ and $V_{max}$, respectively. When the isotope effects are near unity, the global fits described by eqs 7–9 gave large errors in the isotope effects. In such cases (e.g., WT IDH1), the NADPH(D) data were fit separately to eq 1 and the isotope effects were calculated from the appropriate ratios with errors propagated by standard rules for division.

**Determination of NADPH $K_d$ Values by Stopped-Flow Fluorescence Spectroscopy.** The kinetic analyses of binding of NADPH to IDH1 enzymes depleted of cofactors were performed using an Applied Photophysics model SX-20 stopped-flow spectrometer. NADPH binding was monitored by the increase in the fluorescence between unbound and bound NADPH by exciting the NADPH at 340 nm and observing the changing emission above 400 nm using a 400 nm cutoff filter. In a typical experiment, 400 nM cofactor-depleted IDH1 was mixed with an equal volume of varied NADPH concentrations in 0.1 M Tris (pH 8.0) containing 10 mM $MgCl_2$. A total of 10000 points were collected in each trace, and for faster time courses with lower signal amplitudes, two or three individual traces were averaged. The reaction mixture and all reagents were thermostated at 25 °C with a circulating water bath.

## RESULTS AND DISCUSSION

Since 2008, frequent somatic mutations in IDH1 and IDH2 have been identified in a wide variety of cancer types. A common theme for these mutations is the neomorphic gain of


dx.doi.org/10.1021/bi400514k | Biochemistry 2013, 52, 4563–4577

Table 1. IDH1 Oxidative Kinetics of Isocitrate to αKG

| construct | $V_{max}$ ($min^{-1}$) | $K_{isocitrate}$ ($\mu M$) | $V/K_{isocitrate}$ ($\mu M^{-1}$ $min^{-1}$) | $K_{NADP^+}$ ($\mu M$) | $V/K_{NADP^+}$ ($\mu M^{-1}$ $min^{-1}$) |
|---|---|---|---|---|---|
| WT/WT | 517 ± 9 | 5.0 ± 0.3 | 103 ± 6 | 6.2 ± 0.3 | 83 ± 4 |
| R132H/R132H | 7.7 ± 0.4 | 6600 ± 860 | 0.0012 ± 0.0002 | 0.055 ± 0.018 | 140 ± 46 |
| G97D/G97D | 58.1 ± 3.5 | 296 ± 75 | 0.20 ± 0.05 | 0.46 ± 0.06 | 126 ± 20 |
| Y139D/Y139D | 0.71 ± 0.02 | 2.4 ± 1.0 | 0.29 ± 0.12 | 0.011 ± 0.003 | 63 ± 18 |
| G97N/G97N | 6.1 ± 0.3 | 0.46 ± 0.07 | 13 ± 2 | 0.60 ± 0.03 | 10.2 ± 0.5 |

function that results in an elevated level of 2HG production. Though the correlation between mutational status and an elevated 2HG level is well established, it is less clear how the mutation directly enables this novel gain of function. Our understanding may be limited by the exclusive use of the R132H mutant for previous studies, as structural and kinetic differences between the wild-type and R132H IDH1 enzymes may simply be a consequence of the mutation and unrelated to the production of 2HG. To broaden our understanding of the causes of 2HG production by IDH1 enzymes, we have examined kinetically and structurally enzymes with mutations at three different positions to look for commonalities.

Published structural studies of the closed, active form of R132H IDH1 with αKG bound revealed few changes in the active site compared with the wild-type/isocitrate enzyme. An exception was the movement of Y139, which is able to more closely approach the substrate portion of the active site in the absence of the C3 isocitrate carboxylate group. On the basis of IDHs from other organisms, this residue plays a key role in promoting the acid/base enolization chemistry of the wild-type enzyme,[29] and it was suggested that its movement in R132H could facilitate direct hydride transfer to the C2 carbonyl of αKG and enhance 2HG production.[30]

To test this hypothesis, we determined the substrate-bound structures of the previously described wild-type and R132H homodimers along with analogous structures for the other 2HG-producing mutants G97D, G97N, and Y139D. G97D was initially identified in a colorectal cancer cell line, while Y139D is a mutant based on mechanistic predictions.[31,32] G97N is a newly discovered mechanistic 2HG-producing mutant, described in this work.

The overall structures of the mutants show little differences among themselves and by comparison with the wild-type IDH1 as indicated by the rms difference between Cα atoms upon superposition of the two molecules of the IDH1 dimers of between 0.29 and 0.40 Å. In the substrate pocket of the R132H homodimer, the previously described rotation of the Y139 side chain around the Cα−Cβ bond was again observed (Figure 1A). As a result, the tyrosine hydroxyl group of Y139 is 3.6 Å from the αKG's Cβ atom and pointing directly at the substrate. By contrast, in the G97D and G97N structures, the side chain of Y139 is in the same position as in the wild-type enzyme (Figure 1B), because residues larger than glycine at position 97 would sterically clash with the alternate conformation of Y139. The H-bond between the OH group of Y139 and D275 is exactly the same length regardless of whether Y139 rotates because of the rotation of the side chain of D275 that follows the displacement of Y139's side chain. In the structure of Y139D, there are no notable conformational rearrangements, though the substitution itself creates a longer distance between the side chain and the substrate binding site, compared with those of the wild-type, G97D, and G97N structures (Figure 1C). Thus, in the various neomorphic mutants, the distance between residue 139 and the substrate is shorter than (R132H), unchanged from (G97D and G97N), or longer than (Y139D) the distance in the wild-type enzyme, leading to the conclusion that this is not a factor in the enhanced production of 2HG.

The binding of NADP/H to IDH1 involves a number of hydrogen bonds and van der Waals contacts between the cofactor and enzyme.[33] On the adenine portion of the cofactor, key interactions with V312, R314, and H315 from subunit A and D253, N257, and K260 from subunit B are formed, while the nicotinamide ring is coordinated by T75, T77, and R82, among others. An overlay of the wild-type and mutant IDH1 structures centered on this site (Figure 1D) reveals the conservation of these interactions and the conformation of the bound NADP/H. In summary, there are no consistent changes to either the substrate or cofactor binding sites in the structures of R132H, G97D, G97N, and Y139D that would readily explain how the mutant enzymes take on the neomorphic ability to produce 2HG.

With respect to kinetics, it has been previously demonstrated that one function of the R132H mutation is to make the conversion of αKG to 2HG more favorable in IDH1 by virtue of decreasing the competitive binding and turnover of isocitrate. This was evidenced by an ∼1000-fold increase in isocitrate $K_i$ and $K_m$ values as well as a 100-fold decrease in $k_{cat}$ with the R132H enzyme.[34] Structurally, this was rationalized by the removal of a stabilizing, positively charged residue in the proximity of the negatively charged isocitrate. A similar explanation can account for the G97D and Y139D mutations, where substitutions result in an increase in destabilizing, negatively charged residues in the same area of the active site.

To further test this hypothesis, we investigated substitutions at G97 and Y139 as well as two other proximal active site residues, N96 and I215. We reasoned that introduction of either an Asp or a Glu at these positions should have effects similar to those of Y139D and G97D. However, none of these mutant enzymes displayed an enhanced neomorphic activity relative to that of the wild-type enzyme, though most displayed the same low level 2HG producing ability as the wild-type enzyme indicating correctly folded protein (Table 2 of the Supporting Information).

We next mutated G97 and Y139 to a wide variety of amino acids, hoping to encompass changes in shape, charge, and hydrophobicity (Table 2 of the Supporting Information). One of these mutations, G97N, displayed an enhanced rate of 2HG production relative to that of the wild-type enzyme, as estimated by comparisons of specific activity. As noted before, the structure of this mutant displayed few noticeable differences from G97D. This mutant does not change the electrostatic nature of the active site and would not be expected *a priori* to affect isocitrate binding.

To further explore this idea, we determined the steady state kinetic parameters of the isocitrate to αKG reaction with the wild-type and four neomorphic IDH1 enzymes (Table 1). Unlike R132H, we found that other 2HG-producing mutant forms of IDH1 still displayed efficient utilization of isocitrate.


dx.doi.org/10.1021/bi400514k | *Biochemistry* 2013, 52, 4563−4577

**Scheme 1. Reductive Chemistries of IDH1**

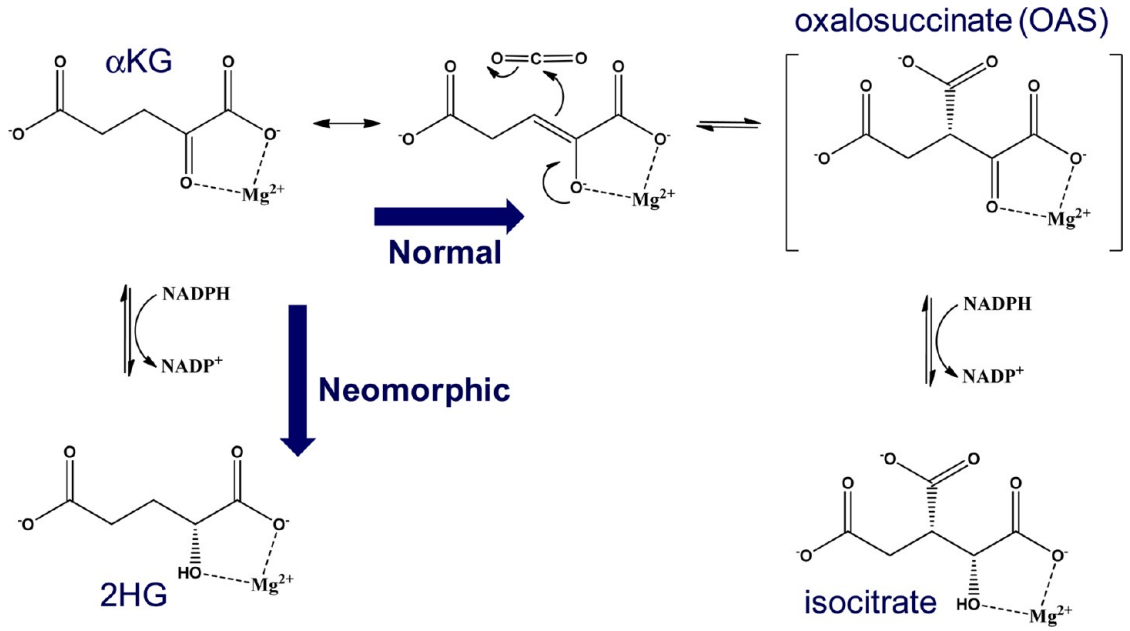


For example, the isocitrate $K_m$ values of 2.4 and 0.5 $\mu$M found with Y139D and G97N, respectively, are both lower than that of the wild-type enzyme (7 $\mu$M), and these enzymes display $V/K_m$ (isocitrate) values 100−10000-fold higher than that of the R132H enzyme. In particular, the $V/K_m$ (isocitrate) for G97N was within 8-fold of that of the wild-type enzyme. From these data, we can conclude that mutations that result in an elevated level of 2HG production do not rely solely on impaired kinetic utilization of isocitrate, as previously proposed.

Because these experiments did not identify a consistent structural variation or kinetic theme common to the 2HG-producing mutants of IDH1, we studied the details of the reductive chemistry catalyzed by both the wild-type and mutant IDH1 enzymes. Among the three mammalian classes of isocitrate dehydrogenases, only the NADP/H utilizing cytosolic (such as human IDH1) and mitochondrial (such as human IDH2) forms have been shown to be capable *in vitro* of reversing $\alpha$KG back to isocitrate, a reductive carboxylation reaction. It has been postulated that this reaction cannot be observed with the NAD/H-utilizing mitochondrial enzymes (such as human IDH3) because of high $K_m$ values for $CO_2$ and $\alpha$KG with this isoform, as demonstrated with the porcine enzyme.[35]

In a similar vein, it has recently been shown that the wild-type forms of IDH1 and IDH2 can catalyze the reductive carboxylation of $\alpha$KG *in vivo*. Cells with impaired mitochondrial respiration, which can occur through mutations in electron transport components or under hypoxic conditions, switch from glucose to glutamine as a primary source of energy and molecular building blocks. Both IDH1 and IDH2, but not IDH3, have been shown to contribute to this process by virtue of their ability to convert $\alpha$KG to isocitrate.[36,37] Interestingly, though these cells are wild-type for IDH1 and IDH2, the increased flux through this reductive pathway also results in a slightly elevated level of 2HG production,[38] consistent with the recent proposal that the typically small amount of this metabolite found in cells may be evolved from the wild-type forms of IDH1 and/or IDH2.[34]

Upon comparison of the reductive mechanisms catalyzed by the wild-type or mutant IDH1 enzymes (Scheme 1), a key difference is the ability of $\alpha$KG to react with $CO_2$ to produce the intermediate oxalosuccinate (OAS).[39] In the wild-type enzyme, this requires enolization of $\alpha$KG and the binding and orientation of $CO_2$ for the reaction. In theory, disruption of either of these processes would result in a switch in product distribution from isocitrate to 2HG, because the subsequent stereospecific reduction of the C2 carbonyl by NADPH is common to both the normal and neomorphic conversions.

To generate testable hypotheses of where $CO_2$ might bind to the enzyme, we performed an *in silico* simulation using the multifragment search technique[28] on the substrate-bound structure of wild-type IDH1 as implemented in MOE from CCG. In this method, the active site is flooded with $CO_2$ molecules and the program predicts areas where $CO_2$ would cluster. One such area defined a contiguous region extending from the interior of the active site proximal to isocitrate out to the surface of the enzyme (Figure 2A). In the wild-type structure, G97 (light green in Figure 2A) lies along a narrow part of this channel, such that mutation to larger residues would be predicted to occlude access to the active site. This can be seen in the structure for G97N (Figure 2B), where the proposed $CO_2$ channel is blocked by the larger asparagine side chain. Consistent with the idea that the 2HG-enhancing mutations share a role in diminishing the level of binding or utilization of $CO_2$ as a substrate, two of the other pro-neomorphic residues, R132 and Y139, represent a known carbon dioxide binding dyad observed in the structures of *E. coli* phosphoenolpyruvate carboxylase enzymes, where they help to orient and polarize $CO_2$ for reaction.[40]

To test this hypothesis, a series of mutations in residues surrounding this proposed channel were made and assayed for enhanced 2HG production. As a general theme, we introduced either negatively charged or large, nonpolar residues in an attempt to inhibit access of $CO_2$ to the active site of IDH1 (Table 3 of the Supporting Information). However, none resulted in a significant (>3-fold) increase in the level of 2HG production, as estimated from specific activity. Though this


dx.doi.org/10.1021/bi400514k | *Biochemistry* 2013, 52, 4563−4577

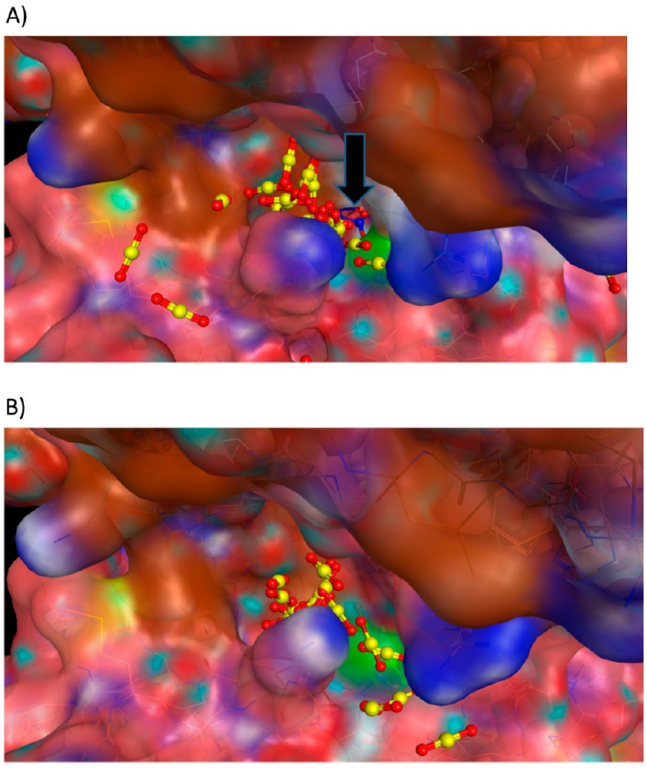


**Figure 2.** Predicted $CO_2$ binding channel. MFSS methods were used to generate a potential binding surface for $CO_2$ in (A) wild-type IDH1 that extends from the surface into the active site, as indicated by the black arrow. Isocitrate is colored blue. This surface is occluded in the model with (B) G97N, where N97 (green) blocks access to isocitrate.

appears to contradict the hypothesis that the shared trait among the neomorphic forms of IDH1 is their decreased ability to utilize $CO_2$ as a substrate, we do not possess a ready experimental method to confirm that these $CO_2$ channel mutants actually impeded the availability of $CO_2$ to the active site.

To further test this idea, we sought an alternative method to assess the contribution that $CO_2$ binding makes to the partitioning of $\alpha$KG to either isocitrate or 2HG. Using wild-type IDH1, we varied the concentration of $CO_2$ in reaction mixtures containing 100 nM enzyme and saturating levels of $\alpha$KG and NADPH and used mass spectrometry methods to quantify the levels of each product (Figure 3). Under saturating (>1 mM) concentrations of added $CO_2$, isocitrate was formed at a high rate (3700 ± 200 nM/min) compared with the rate of 2HG production (10.7 ± 0.5 nM/min). As the concentration of added $CO_2$ in the reaction mixture was reduced below its $K_m$ of ~0.6 mM, the rate of isocitrate formation decreased significantly, reaching a minimum of 62 ± 4 nM/min.

In these same reactions with a decreasing level of $CO_2$, we observed a consistent trend of increasing rates of 2HG production (Figure 3). However, the magnitude of this effect was only ~2-fold, and the resultant rate (0.24 ± 0.01 $min^{-1}$) was far short of the previously reported values for R132H.[34] Thus, we conclude from this experiment that while limiting the ability of IDH1 to use $CO_2$ as a substrate may contribute to the overall gain in ability to produce 2HG, the much larger increase observed with mutant forms of the enzyme must have additional contributions from other sources.

We also attempted to make changes to IDH1 that might result specifically in impaired enolization of $\alpha$KG, through

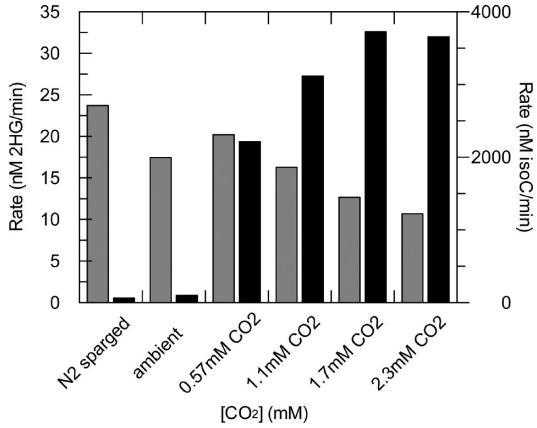


**Figure 3.** Product distribution as a function of $CO_2$ concentration. The conversion of $\alpha$KG to either isocitrate (black bars) or 2HG (gray bars) was monitored by liquid chromatography and mass spectrometry of reaction mixtures containing 100 nM homodimeric wild-type IDH1, 200 $\mu$M NADPH, 5 mM $\alpha$KG, and varying concentrations of $CO_2$.

mutations of the canonical acid/base pair in this family of enzymes,[29] Y139 and K212. However, except for the Y139D enzyme, none of these changes resulted in an increased level of 2HG production by IDH1 (Table 2 of the Supporting Information).

We next turned our attention to the utilization of $\alpha$KG and NADPH as substrates by the wild-type (with added $CO_2$) and mutant forms (in the absence of $CO_2$) of IDH1. In previous kinetic studies of R132H IDH1, it had been noted that the enzyme displays a relatively weak affinity for $\alpha$KG and a strong affinity for NADPH.[34] To test the generality of these results, we determined the reductive steady state kinetics of the wild-type, R132H, G97D, G97N, and Y139D homodimeric enzymes (Table 2). For the wild-type enzyme, a $V/K_m$ ($\alpha$KG) value of 0.97 ± 0.27 $\mu M^{-1}$ $min^{-1}$ was obtained under saturating concentrations of the cosubstrates. Among the various 2HG-producing mutants studied, all displayed significantly reduced catalytic efficiencies, with values only 1−4% of that of the wild-type enzyme.

Historically, obtaining an accurate determination of the NADPH kinetics with R132H has been challenging because of the unusually low $K_m$ value for this substrate.[15,34] While only limiting values for the NADPH $K_m$ had previously been reported using spectroscopic or fluorometric techniques, we used more sensitive mass spectrometry methods to extend the window of 2HG detection and determine these values more accurately. We found that while the wild-type enzyme displays a $K_m$ for NADPH in the range of 50−100 $\mu$M, the values for all of our mutants were consistently <500 nM, representing a >100-fold decrease in this parameter (Table 2). In all cases, the lower $K_m$ (NADPH) for the mutant enzymes resulted in enhanced $V/K_m$ (NADPH) values, though the magnitude ranged from modest (3-fold for Y139D) to large (46-fold for R132H). Thus, compared with the wild-type enzyme, the neomorphic mutants share the common trend of increased catalytic efficiency with NADPH and decreased efficiency with $\alpha$KG.

It should be noted that the $K_m$ values for NADPH are kinetic in nature and do not necessarily correspond to a greater affinity. To probe this point further, we sought to determine the dissociation constant of NADPH by direct methods. Complicating this experiment is the fact that the cofactor


dx.doi.org/10.1021/bi400514k | *Biochemistry* 2013, 52, 4563−4577

**Table 2. IDH1 Reductive Kinetics and Steady State and Dead-End Inhibition Summary**

| construct | varied substrate | $V_{max}$ ($min^{-1}$)[a] | $K_m$ ($\mu M$)[a] | $V/K_m$ ($\mu M^{-1} min^{-1}$) | fixed substrate[b] | inhibitor | inhibition type[c] | $K_{is}$ ($\mu M$)[a] | $K_{ii}$ ($\mu M$)[a] |
|---|---|---|---|---|---|---|---|---|---|
| WT/WT | αKG | 134 ± 5 | 138 ± 38 | 0.97 ± 0.27 | NADPH (200 μM), $CO_2$ (2.28 mM) | N-OG | C | 116 ± 32 | |
| WT/WT | NADPH | 137 ± 6 | 60.2 ± 8.2 | 2.28 ± 0.33 | αKG (0.5 mM), $CO_2$ (2.28 mM) | N-OG | NC | 3780 ± 401 | 3780 ± 401 |
| WT/WT | $CO_2$ | 121 ± 6 | 636 ± 79 | 0.19 ± 0.03 | NADPH (200 μM), αKG (0.5 mM) | N-OG | NC | 2240 ± 195 | 2240 ± 195 |
| WT/WT | NADPH | 164 ± 8 | 47.2 ± 8.4 | 3.47 ± 0.64 | αKG (0.5 mM), $CO_2$ (2.28 mM) | $NAADP^+$ | C | 520 ± 96 | |
| WT/WT | αKG | 86.2 ± 2.1 | 381 ± 24 | 0.23 ± 0.02 | NADPH (50 μM), $CO_2$ (2.28 mM) | $NAADP^+$ | NC | 4800 ± 475 | 4800 ± 475 |
| WT/WT | $CO_2$ | 94.2 ± 4.6 | 666 ± 85 | 0.14 ± 0.02 | NADPH (50 μM), αKG (0.5 mM) | $NAADP^+$ | NC | 415 ± 110 | 920 ± 249 |
| R132H/R132H | αKG | 42.8 ± 0.7 | 1080 ± 67 | 0.040 ± 0.003 | NADPH (50 μM) | N-OG | C | 103 ± 6 | |
| R132H/R132H | NADPH | 45.0 ± 0.9 | 0.43 ± 0.04 | 105 ± 10 | αKG (1 mM) | N-OG | UC | | 223 ± 11 |
| R132H/R132H | NADPH | 30.7 ± 0.8 | 0.30 ± 0.04 | 102 ± 14 | αKG (1 mM) | $NAADP^+$ | C | 3.11 ± 0.56 | |
| R132H/R132H | αKG | 31.9 ± 1.3 | 1330 ± 137 | 0.024 ± 0.003 | NADPH (0.5 μM) | $NAADP^+$ | NC | 15.1 ± 1.4 | 15.1 ± 1.4 |
| G97D/G97D | αKG | 3.25 ± 0.06 | 218 ± 11 | 0.015 ± 0.001 | NADPH (50 μM) | N-OG | C | 31.6 ± 1.3 | |
| G97D/G97D | NADPH | 2.38 ± 0.03 | 0.25 ± 0.02 | 9.52 ± 0.77 | αKG (0.2 mM) | N-OG | UC | | 47.3 ± 1.9 |
| Y139D/Y139D | αKG | 1.04 ± 0.01 | 74.2 ± 3.8 | 0.014 ± 0.001 | NADPH (50 μM) | N-OG | C | 17.2 ± 0.8 | |
| Y139D/Y139D | NADPH | 1.01 ± 0.02 | 0.16 ± 0.01 | 6.31 ± 0.41 | αKG (0.2 mM) | N-OG | UC | | 73.6 ± 3.7 |
| G97N/G97N | αKG | 2.52 ± 0.05 | 295 ± 13 | 0.0090 ± 0.0004 | NADPH (50 μM) | N-OG | C | 88.9 ± 3.6 | |
| G97N/G97N | NADPH | 1.95 ± 0.04 | 0.11 ± 0.01 | 17.7 ± 1.7 | αKG (0.4 mM) | N-OG | UC | | 307 ± 18 |

[a] $V_{max}$, $K_m$, and $K_{is}$ values are best determined from competitive fits at saturating fixed substrate concentrations. $K_{is}$ is the slope inhibition constant, and $K_{ii}$ is the intercept inhibition constant. [b] At pH 8 100 mM $NaHCO_3$ equals 2278 μM $CO_2$. [c] Abbreviations: C, competitive; NC, noncompetitive; UC, uncompetitive.

**Table 3. Cofactor Stoichiometry**

| | Amount of $NADP^+$/H Bound to IDH1 Enzymes | | | | | |
|---|---|---|---|---|---|---|
| | pretreatment | | | post-treatment | | |
| construct[a] | [IDH1] (μM) | [$NADP^+$] (μM) | [NADPH] (μM) | [IDH1] (μM) | [$NADP^+$] (μM) | [NADPH] (μM) |
| WT/WT | 10 | 3 | 6 | 50 | 4.9 | 0.4 |
| R132H/R132H | 10 | <1 | 7.8 | 40 | <1 | <0.25 |
| G97D/G97D | 20 | <1 | 25 | 50 | <1 | <0.25 |
| G97N/G97N | 10 | 1.6 | 8.7 | 50 | <1 | <0.25 |
| Y139D/Y139D | 10 | 2.7 | 7.1 | 50 | <1 | <0.25 |

[a] Limits of detection = 1 μM for $NADP^+$ and 0.25 μM for NADPH.

typically co-purifies with either wild-type or mutant enzyme.[30] This challenge has been found in studies with other dehydrogenases and has been overcome by incubating the enzyme with the cosubstrate to turn over the cofactor to a less tightly bound product form.[41] We determined the amount of $NADP^+$ and NADPH bound to our purified IDH1 enzymes and found that they contained nearly stoichiometric amounts, primarily in reduced form (Table 3). After incubation with excess cosubstrate and repurification, we were able to remove >90% of the cofactor from all enzymes, resulting in a form of IDH1 suitable for direct binding experiments.

Using this cofactor-free form of IDH1, NADPH binding kinetics were measured by changes in ligand fluorescence on a stopped-flow apparatus (Figure 4A). By varying the concentration of NADPH in the presence of fixed concentrations of each of the IDH1 mutants, observed binding rate constants ($k_{obs}$) were determined from single-exponential fits. These fits were then replotted to determine the on and off rate constants for NADPH and calculate the $K_d$ for the ligand (Figure 4B and Table 4). The linear replots also indicate a single-step binding mechanism and simplify the calculation of $K_d$ to $k_{off}/k_{on}$. From the plot in Figure 4B, an off rate constant of 0.33 ± 0.07 $s^{-1}$ and an on rate constant of 7.7 ± 0.1 $\mu M^{-1}$ $s^{-1}$ could be fit and a calculated $K_d$ value of 43 ± 9 nM determined for binding of NADPH to R132H IDH1. Similar tight binding of NADPH was calculated for G97D (13 ± 6 nM), Y139D (120 ± 27 nM), and G97N (13 ± 6 nM). The especially tight binding of NADPH to the G97D and G97N enzymes was a function of a faster on rate constant, as all mutants displayed similar off rate constants (~1 $s^{-1}$).

For the wild-type enzyme, the calculation of on and off rate constants was complicated by the need to fit the primary data to two exponentials (Figure 4C). Most commonly, this phenomenon can be attributed to a single, two-step binding mechanism. However, upon replotting the data, we observed that both processes displayed a linear dependence on NADPH concentration, indicating two separate bimolecular processes. In the case of a single two-step binding event, a ligand-independent rate would have been observed because of the unimolecular nature of the second binding step.[41] The more complex binding kinetics observed with wild-type IDH1 may result from a mixture of conformational populations. Consistent with this idea, it has been previously shown that the individual subunits of the wild-type IDH1 homodimer are asymmetric in crystal structures.[33]


dx.doi.org/10.1021/bi400514k | Biochemistry 2013, 52, 4563−4577

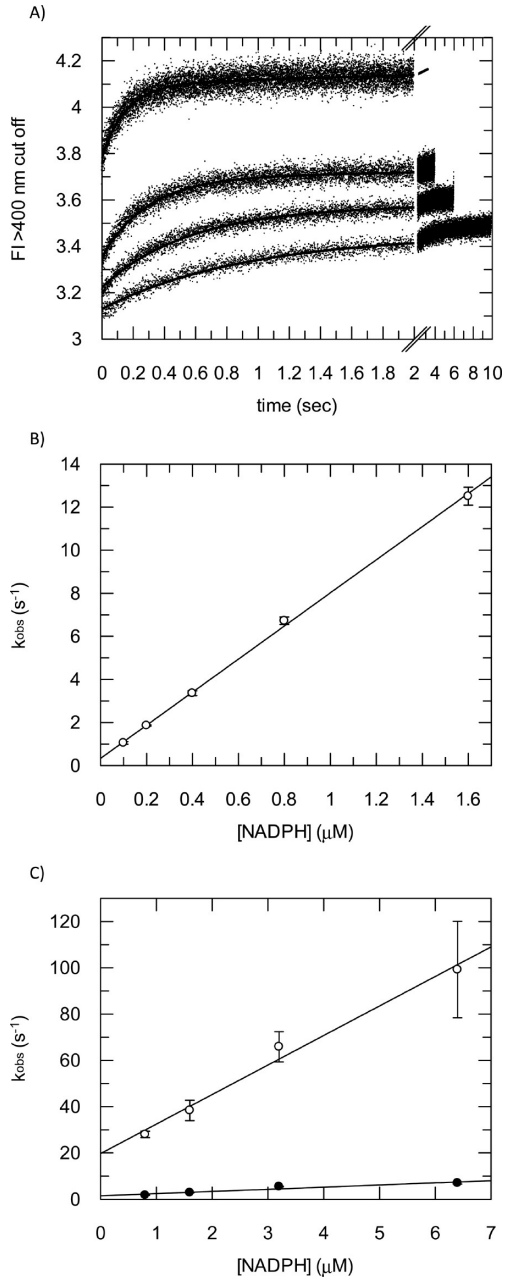


**Figure 4.** Determination of the kinetics of binding of NADPH to IDH1 enzymes. (A) Examples of stopped-flow traces of binding of NADPH to homodimeric R132H IDH1 as monitored by changes in NADPH fluorescence (from top, 0.8 $\mu$M NADPH, to bottom, 0.1 $\mu$M NADPH, with 2-fold increments between them). Traces fit best to a single exponential with a final linear rate for R132H IDH1 (—) and other mutants but to a double exponential for homodimeric wild-type IDH1 (not shown). (B and C) Rates of binding of NADPH to homodimeric R132H (B) or wild-type [C, in which both fast (○), $k_1$, and slow (●), $k_2$, phases are shown] IDH1 as a function of NADPH concentration. Linear fits yielded values for $k_{on}$ (slope) and $k_{off}$ (intercept) with each enzyme. Fitted values are summarized in Table 4.

Using this double-exponential fit, similar $K_d$ values of 1.5 ± 0.4 and 1.6 ± 0.4 $\mu$M could be calculated from the replots of both fast- and slow-phase $k_{obs}$ versus NADPH concentration (Figure 4C). These values are 12−115 times higher than those found for the mutant forms of IDH1, consistent with the relative NADPH $K_m$ values. It should be noted that to avoid bias in this analysis, we also fit the wild-type binding data to a single-exponential equation, despite obvious deviations with the data. Even though this fitting is not appropriate for the data, a $K_d$ value similar to that from the double-exponential fits of 3.2 ± 0.4 $\mu$M was obtained.

On the basis of the observed changes in substrate utilization displayed by the mutant forms of IDH1, we investigated the kinetic mechanisms for the conversion of $\alpha$KG to either isocitrate by wild-type IDH1 or 2HG by the mutant IDH1 enzymes. A kinetic mechanism for the neomorphic reaction has not previously been determined, nor has a mechanism been published for the reductive conversion of $\alpha$KG to isocitrate by the wild-type form of IDH1, which would serve as a useful comparison. The mechanism for the conversion of $\alpha$KG to isocitrate has been extensively studied with the mitochondrial IDH from porcine liver (related to the human IDH2 enzyme), using a combination of product and dead-end inhibition studies as well as equilibrium isotope exchange experiments.[42,43] From the sum of that work, the enzyme was predicted to proceed through a random, sequential mechanism.

We began by performing dead-end inhibition studies for wild-type IDH1 similar to those published for the porcine liver enzyme. As an example, we used *N*-oxalylglycine (N-OG) which is a close isostere of $\alpha$KG but behaves as a dead-end inhibitor. In studies with wild-type IDH1, N-OG was found to be a competitive (C) inhibitor with respect to $\alpha$KG and a mixed/noncompetitive (NC) inhibitor with respect to NADPH (Figure 5A,B). These data are summarized in Table 2 and are in accord with wild-type IDH1 proceeding through a random mechanism with respect to $\alpha$KG and NADPH.

We next repeated these studies with the R132H homodimer as a sentinel for the other mutant forms of IDH1. Cotitration of substrates led to a series of intersecting lines in a double-reciprocal plot, consistent with a sequential mechanism (Figure 6A), similar to that of the wild-type enzyme. However, in repeating the pattern of inhibition with N-OG, we began to observe differences between the mutant and wild-type IDH1. With R132H, N-OG remained a competitive inhibitor with respect to $\alpha$KG but displayed an uncompetitive pattern when covaried with NADPH (Figure 6B). The finding of an uncompetitive pattern is typically associated with an ordered kinetic mechanism, and this pattern specifically suggests that NADPH is bound first and $\alpha$KG second to form the active, ternary complex. This order of binding would make sense given the increased catalytic efficiency of the mutant enzymes toward NADPH and decreased efficiency toward $\alpha$KG.

Given that the changes in substrate utilization were displayed by all of the neomorphic IDH1 mutants, we were interested in whether a similar apparent change in mechanism would be found with the G97D, G97N, and Y139D forms of the enzyme. Repeating the cotitrations of N-OG and NADPH with these enzymes yielded similar uncompetitive patterns as determined for R132H (Figure 6C−E and Table 2).

As previously mentioned, the finding of an uncompetitive pattern of inhibition is most easily reconciled with an ordered kinetic mechanism, although another possibility that would account for the observed data with N-OG is a random mechanism with a very low $\alpha$ value for binding of the second substrate.[44] In this case, N-OG would still be considered a mixed-type inhibitor with NADPH but simply display a very strong uncompetitive component, yielding a series of lines in the replot that would eventually converge if extended sufficiently. One piece of evidence that conflicts with this


dx.doi.org/10.1021/bi400514k | *Biochemistry* 2013, 52, 4563−4577

**Table 4. NADPH Binding Parameters Determined by Stopped-Flow Fluorescence**

| | single-exponential fit | | | double-exponential fit | | |
|---|---|---|---|---|---|---|
| construct | $k_{on}$ ($\mu M^{-1}$ $s^{-1}$) | $k_{off}$ ($s^{-1}$) | $K_d$ ($\mu M$) | $k_{on}$ ($\mu M^{-1}$ $s^{-1}$) | $k_{off}$ ($s^{-1}$) | $K_d$ ($\mu M$) |
| R132H/R132H | 7.69 ± 0.091 | 0.331 ± 0.067 | 0.043 ± 0.0087 | | | |
| G97D/G97D | 115 ± 3.7 | 1.50 ± 0.701 | 0.013 ± 0.0061 | | | |
| Y139D/Y139D | 11.6 ± 0.36 | 1.39 ± 0.31 | 0.12 ± 0.027 | | | |
| G97N/G97N | 91.9 ± 3.5 | 1.16 ± 0.502 | 0.013 ± 0.0055 | | | |
| WT/WT[a] | 5.53 ± 0.81 | not determined | 3.15 ± 0.43 | | | |
| WT/WT | 12.8 ± 1.32 | 19.7 ± 5.01 | 1.5 ± 0.41 | 0.935 ± 0.0849 | 1.53 ± 0.322 | 1.6 ± 0.37 |

[a]Binding of NADPH to WT/WT IDH1 fit best to a double exponential. An off rate could not be determined using a single-exponential fit.

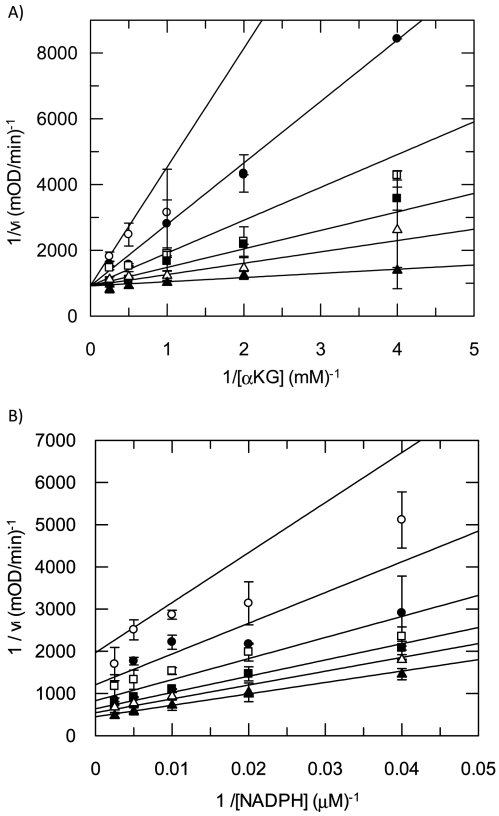


**Figure 5.** Patterns of dead-end inhibition indicate a random, sequential kinetic mechanism for wild-type IDH1. (A) Competitive, dead-end inhibition is observed between N-OG [3.2 (○), 1.6 (●), 0.8 (□), 0.4 (■), or 0.2 mM (△) or no inhibitor (▲)] and $\alpha$KG in reactions catalyzed by homodimeric wild-type IDH1. (B) Mixed/noncompetitive, dead-end inhibition is observed between N-OG [12.8 (○), 6.4 (●), 3.2 (□), 1.6 (■), or 0.8 mM (△) or no inhibitor (▲)] and NADPH in reactions catalyzed by homodimeric wild-type IDH1. Rate data from the figure are reported as mOD at 340 nm per minute and converted to turnover numbers in Table 2 using an NADPH standard curve. Lines are from data fit to the appropriate equations with parameters summarized in Table 2.

possibility is the substrate cotitration (Figure 6A), which when fit to a random model resulted in an $\alpha$ value of 0.27, within 4-fold of unity and much larger than the value needed to yield the observed N-OG inhibition patterns with the mutant IDH1 enzymes. Another argument against this mechanism is the finding of clearly mixed/noncompetitive inhibition in the other complementary pair of dead-end inhibition studies, between the NADPH competitive inhibitor $NAADP^+$ and $\alpha$KG using the R132H enzyme (Table 2). If a random mechanism with a low $\alpha$ value were operative, we would have expected to find the same apparent uncompetitive pattern when covarying these species.

As yet another way to confirm the ordered mechanism for the neomorphic IDH1 enzymes, we measured the effect of varying the concentration of $\alpha$KG on the $^D(V/K)$ for NADPH. In multisubstrate reactant systems, saturation with a second substrate will have differing effects on the isotope effect of the first substrate depending on the kinetic mechanism.[45] In an ordered mechanism, saturation with the second binding substrate can fully commit the enzyme forward and thus reduce the $^D(V/K)$ for the first binding substrate to unity from its observed value at subsaturating concentrations. However, the converse is true in a random mechanism, and the $^D(V/K)$ will persist even as the second substrate is saturated.

To conduct these experiments, we used the structure of the R132H homodimer to predict that the pro-*R* hydrogen of the NADPH nicotinamide ring is transferred to $\alpha$KG during the reductive reaction that produces 2HG. Using the alcohol dehydrogenase from *T. brockii*, we exchanged the pro-*R* hydrogen for deuterium using $d_8$-2-propanol as a source of the label.[20] In parallel, we conducted a similar reaction using unlabeled 2-propanol to generate a matched pair of NADPH and NADPD to use in the isotope effect studies.

We conducted these experiments using Y139D in place of R132H, given the lower $K_m$ of Y139D for $\alpha$KG, thus making it easier to saturate with this substrate. At 1.3-fold $K_m$ concentrations of $\alpha$KG, Y139D displayed $^DV = {}^D(V/K)_{NADPH} = 3.5 \pm 0.4$ (Figure 7A). This value is at the upper limit reported for dehydrogenases[46] and indicates that hydride transfer is largely rate-limiting. We repeated the determination of $^D(V/K)_{NADPH}$ under saturating conditions, where the $\alpha$KG concentration equals 133-fold $K_m$. Under these conditions, $^D(V/K)_{NADPH}$ was reduced to unity (Figure 7B), while $^DV$ remained high (3.8). Similar results were obtained with G97D, where $^D(V/K)_{NADPH}$ was reduced from 3.0 ± 0.2 to unity upon saturation with $\alpha$KG (Table 5). This result, like the dead-end inhibition studies, is most consistent with an ordered mechanism for the neomorphic forms of IDH1 with NADPH binding preceding $\alpha$KG.[a]

As a corollary to these isotope studies, in an ordered mechanism, $^D(V/K)$ for the second substrate is independent of the concentration of the first substrate. For each of the mutant enzymes, saturating with cofactor resulted in no diminution of the maximal isotope effect on $^D(V/K)$ for $\alpha$KG (Table 5).

It should be noted that all of the 2HG-producing mutant IDH1 enzymes displayed similar primary isotope effects on both $V$ and $V/K$ in contrast to the wild-type enzyme, which did not display an effect; i.e., $^DV = {}^D(V/K) = 1$ (Table 5). The result with wild-type IDH1 is consistent with published studies of the wild-type NADPH-dependent enzyme from porcine heart, where there was a lack of primary deuterium effect in


dx.doi.org/10.1021/bi400514k | *Biochemistry* 2013, 52, 4563−4577

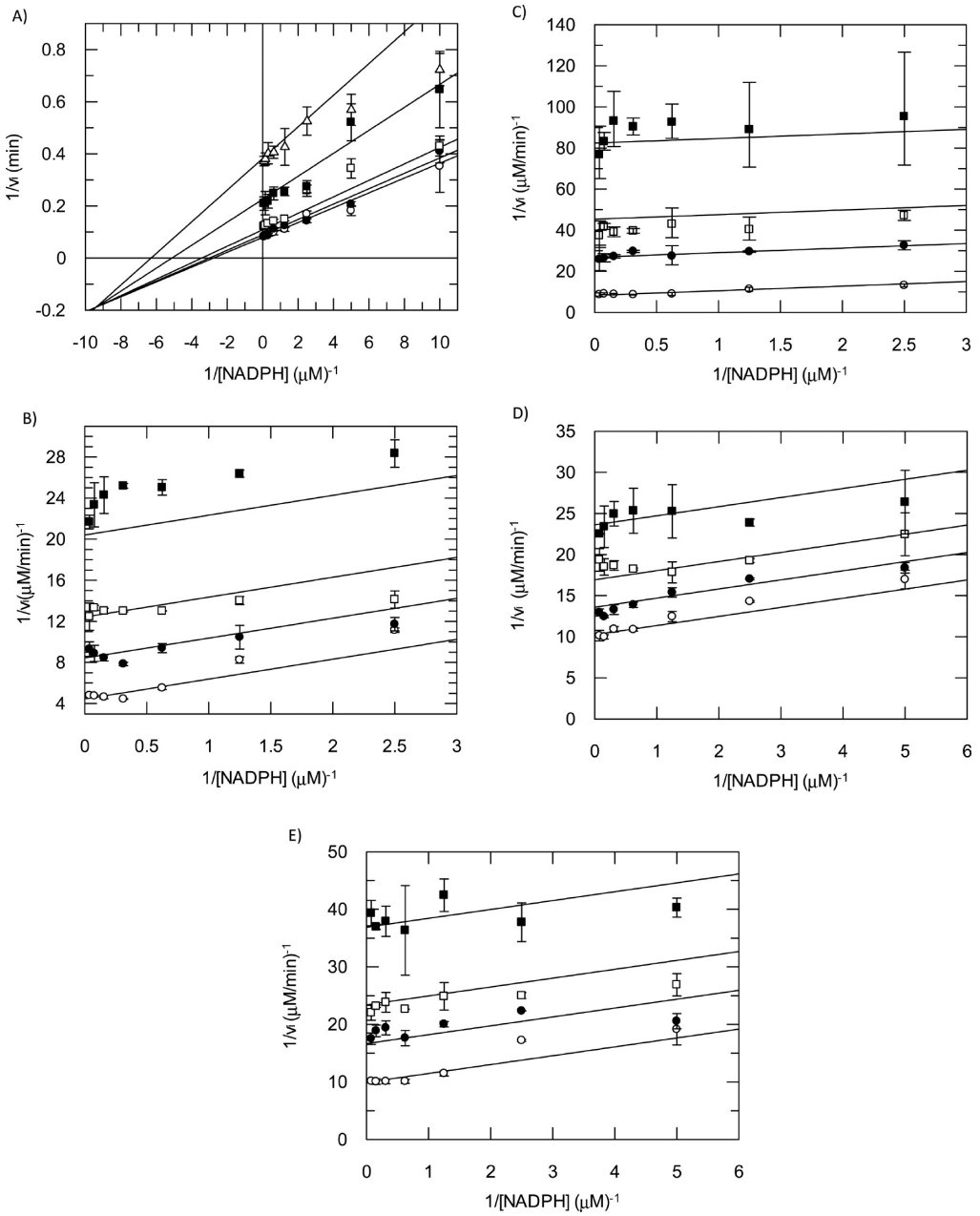


**Figure 6.** Patterns of substrate kinetics and dead-end inhibition indicate an ordered, sequential kinetic mechanism for mutant forms of IDH1. (A) Dual titration of αKG [12.8 (○), 6.4 (●), 3.2 (□), 0.8 (■), and 0.4 mM (△)] and NADPH (from 0.1 to 12.8 μM) demonstrates a sequential mechanism for homodimeric R132H IDH1. Lines are from the fits to eq 2 with the following values: $V_{max}$ = 14.4 ± 0.5 $min^{-1}$; $K_{NADPH}$ = 0.40 ± 0.05 μM; $K_{αKG}$ = 1800 ± 200 μM; $K_{iNADPH}$ = 0.11 ± 0.08 μM ($\alpha$ = 0.27). (B−E) N-OG behaves as an uncompetitive, dead-end inhibitor with NADPH in reactions catalyzed by the homodimeric R132H (at 5 nM), G97D (at 50 nM), G97N (at 50 nM), and Y139D (at 100 nM) IDH1 enzymes. N-OG concentrations were 0.8 (■), 0.4 (□), or 0.2 mM (●) or no inhibitor (○) for R132H; 0.4 (■), 0.2 (□), or 0.1 mM (●) or no inhibitor (○) for G97D and G97N; and 0.2 (■), 0.1 (□), or 0.05 mM (●) or no inhibitor (○) for Y139D. Lines are from duplicate data fit to the appropriate equations with parameters summarized in Table 2.

either the forward or reverse direction[47] and it was found that in the forward direction release of the sticky substrate isocitrate occurs more slowly than chemistry, resulting in the lack of an isotope effect on $^{13}(V/K)_{isocitrate}$.[48]

The change in mechanism for reductive chemistry that accompanies mutation of wild-type IDH1 can help to explain the phenomenon of enhanced 2HG production. In utilizing a random sequential mechanism, the wild-type enzyme is able to elaborate αKG to oxalosuccinate before reduction by NADPH to produce isocitrate. However, in an ordered mechanism with NADPH bound first and tightly, the enzyme is better poised to reductively trap αKG directly to 2HG. This effect, in combination with the reduced ability to utilize $CO_2$ as a substrate, can account for the dramatic increase in the level of 2HG that accompanies these cancer-associated mutations both *in vitro* and *in vivo*.

The mechanism-altering effects of the IDH1 mutations are precedented in other systems. Studies with zeta class glutathione transferase GSTZ1c-1c demonstrated that the C16A mutation led to a change from a random to ordered mechanism.[49] As seen for IDH1, a decrease in affinity was found for one of the GSTZ1c-1c cosubstrates, leading to the


dx.doi.org/10.1021/bi400514k | *Biochemistry* 2013, 52, 4563−4577

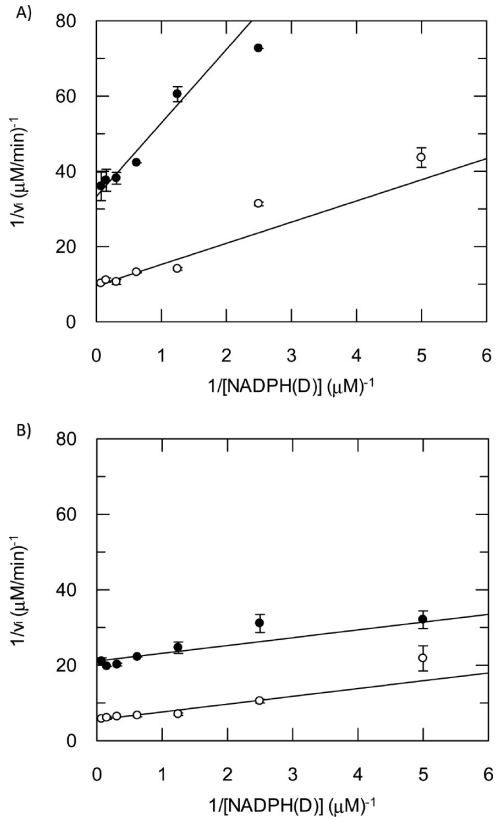


**Figure 7.** Primary isotope effects with mutant forms of IDH1 confirm an ordered binding kinetic mechanism. (A) $V/K_{NADPH}$ was determined for reaction mixtures containing either NADPH (○) or NADPD (●) at 1.3$K_m$ values of αKG (100 μM) with Y139D IDH1. $^{D}V$ and $^{D}(V/K)_{NADPH}$ were calculated using eq 8. (B) $V$ and $V/K_{NADPH}$ were determined for reaction mixtures containing either NADPH (○) or NADPD (●) at 133$K_m$ values of αKG (10 mM) with Y139D IDH1. $^{D}V$ and $^{D}(V/K)_{NADPH}$ values (=1.0) were calculated using eq 9.

altered order of substrate binding. Also in analogy to IDH1, a recent kinetic characterization of the wild-type and a triclosan resistant T276S mutant of *Yersinia pestis* FabV was described, where the mutation led to a change from a random to an ordered mechanism, with NADH binding first.[50]

Though our kinetic results with the wild-type and mutant IDH1 enzymes help us to better understand the connection between the cause and effect of the mutations and 2HG production, it should be recognized that several of the IDH1 enzymes in this study are capable of catalyzing both the normal and neomorphic reactions, to varying degrees. This includes wild-type IDH1, which has been previously shown to be able to form 2HG, albeit at a rate greatly reduced compared with the mutant enzymes.[34] We performed preliminary studies of this reaction and determined that wild-type IDH1 displays a very low (<200 nM) $K_m$ for NADPH and a finite $^{D}V_{αKG}$ of 3.5 ± 0.43 equal to $^{D}(V/K)_{αKG}$ at a saturating NADPH(D) concentration (buffers sparged with $N_2$ to minimize $CO_2$) when monitoring 2HG production by LC-MS/MS instead of isocitrate. These results would be consistent with a change in mechanism, though confirming this through the types of dead-end inhibition and isotope effect studies described for the mutant enzymes is not possible because of the large amount of wild-type enzyme needed to evolve sufficient levels of 2HG for detection; i.e., [IDH1] > $K_m$ (NADPH). However, future studies with G97N, for which kinetic measurements of both the normal and neomorphic reactions are possible, may shed further light on how IDH1 partitions αKG and NADPH between different kinetic mechanisms and resulting product distributions.

As mentioned previously, analogous 2HG-enhancing mutations can also be found at R140 and R172 of IDH2. It will be of interest to determine if a similar change in kinetic mechanism accompanies the mutations in this human isoform of isocitrate dehydrogenase.

**Table 5. Primary Kinetic Isotope Parameters**

| construct | parameter (fitted eq) | isotope effect[a] | varied substrate | fixed substrate concentration (ratio [S]/$K_m$)[b] |
|---|---|---|---|---|
| WT/WT[c] | $V_{NADPH}$ (1) | 1.01 ± 0.07 | NADPH(D) | 1 mM αKG (11.6); 2.28 mM $CO_2$ (3.6) |
| WT/WT[c] | $V/K_{NADPH}$ (1) | 0.987 ± 0.210 | NADPH(D) | 1 mM αKG (11.6); 2.28 mM $CO_2$ (3.6) |
| WT/WT[c] | $^{D}V_{αKG}$ (1) | 0.99 ± 0.05 | αKG | 200 μM NADPH(D) (3.3); 2.28 mM $CO_2$ (3.6) |
| WT/WT[c] | $^{D}(V/K)_{αKG}$ (1) | 0.92 ± 0.21 | αKG | 200 μM NADPH(D) (3.3); 2.28 mM $CO_2$ (3.6) |
| R132H/R132H[d] | $V_{NADPH}$, $V/K_{NADPH}$ (8) | 2.12 ± 0.19 | NADPH(D) | 1 mM αKG (0.63) |
| R132H/R132H[c] | $^{D}V_{αKG}$, $^{D}V/K_{αKG}$ (8) | 2.24 ± 0.24 | αKG | 20 μM NADPH(D) (55) |
| G97D/G97D[d] | $^{D}V_{αKG}$, $^{D}V/K_{αKG}$ (8) | 3.04 ± 0.21 | NADPH(D) | 0.1 mM αKG (0.62) |
| G97D/G97D[d] | $V_{NADPH}$ (9) | 2.37 ± 0.20[f] | NADPH(D) | 20 mM αKG (124) |
| G97D/G97D[d] | $V/K_{NADPH}$ (9) | 1[e] | NADPH(D) | 20 mM αKG (124) |
| G97D/G97D[c] | $^{D}V_{αKG}$, $^{D}V/K_{αKG}$ (8) | 2.80 ± 0.18 | αKG | 20 αM NADPH(D) (33) |
| Y139D/Y139D[d] | $^{D}V_{NADPH}$, $^{D}V/K_{NADPH}$ (8) | 3.48 ± 0.37 | NADPH(D) | 0.1 mM αKG (1.3) |
| Y139D/Y139D[d] | $^{D}V_{NADPH}$ (9) | 3.82 ± 0.36 | NADPH(D) | 10 mM αKG (133) |
| Y139D/Y139D[d] | $^{D}V/K_{NADPH}$ (9) | 1[f] | NADPH(D) | 10 mM αKG (133) |
| Y139D/Y139D[c] | $^{D}V_{αKG}$, $^{D}V/K_{αKG}$ (8) | 2.93 ± 0.13 | αKG | 20 μM NADPH(D) (54) |
| G97N/G97N[d] | $^{D}V_{NADPH}$, $^{D}V/K_{NADPH}$ (8) | 2.65 ± 0.15 | NADPH(D) | 0.3 mM αKG (1.4) |
| G97N/G97N[c] | $^{D}V_{αKG}$, $^{D}V/K_{αKG}$ (8) | 2.79 ± 0.11 | αKG | 20 μM NADPH(D) (180) |

[a]Isotope effects were obtained by fitting of duplicate determinations of the initial rate data to the indicated equations with experimental errors arising from the fitting. [b]At pH 8 100 mM $NaHCO_3$ equals 2278 μM $CO_2$. [c]NADPH oxidation monitored spectrophotometrically. [d]2HG determined by LC-MS. [e]The same data fit to eq 1 gave a $^{D}V_{NADPH}$ of 2.41 ± 0.14 and a $^{D}V/K_{NADPH}$ of 0.82 ± 0.21 showing that $^{D}V/K_{NADPH}$ was not significantly different from 1.0. [f]The same data fit to eq 1 gave a $^{D}V_{NADPH}$ of 3.63 ± 0.15 and a $^{D}V/K_{NADPH}$ of 1.54 ± 0.31 showing that $^{D}V/K_{NADPH}$ was not significantly different from 1.0.


dx.doi.org/10.1021/bi400514k | *Biochemistry* 2013, 52, 4563−4577

## ■ ASSOCIATED CONTENT

### Supporting Information

A summary of the crystallization statistics for the R132H, G97D, G97N, and Y139D homodimeric enzymes (Table 1) and relative neomorphic activities (2HG production) for all mutants not included in the text (Tables 2 and 3). This material is available free of charge via the Internet at http://pubs.acs.org.

### Accession Codes

PDB entries 4L06, 4L04, 4L03, and 4KZO for Y139D/Y139D, G97N/G97N, G97D/G97D, and R132H/R132H, respectively.

## ■ AUTHOR INFORMATION


### Corresponding Author

*E-mail: Benjamin.2.Schwartz@gsk.com. Phone: (610) 917-6740. Fax: (610) 917-7385.


### Notes

The authors declare the following competing financial interest(s): We are employees of GlaxoSmithKline.

## ■ ACKNOWLEDGMENTS

We thank Gaochao Tian, Tom Meek, Fan Fan, and Professor W. W. Cleland for helpful experimental suggestions and Ken Wiggall and Karl Erhard for assistance in the synthesis of $d_4$-2HG.

## ■ ADDITIONAL NOTE

[a]The switch to an ordered mechanism for the neomorphic reaction is not simply a reflection of the substantially decreased $K_m$ value for NADPH. Dead-end inhibition studies and NADPH(D) kinetic isotope effects with the homodimeric double mutant, R132H/H315A,[34] which has an elevated NADPH $K_m$ (7 $\mu$M) because of the H315A mutation, produced results similar to those with single-point mutations. That is, N-OG was uncompetitve vs NADPH, and $^{D}(V/K)_{NADPH}$ was reduced from 2.58 ± 0.14 at 0.25 mM $\alpha$KG (0.1-fold $K_m$) to 1.64 ± 0.37 at 25 mM $\alpha$KG (11-fold $K_m$). The double mutant also exhibited a large isotope effect on $V_{max}$ that did not change significantly between low ($^{D}V$ = 2.58 ± 0.14) and high $\alpha$KG ($^{D}V$ = 2.76 ± 0.16) levels. These results are consistent with an ordered mechanism for R132H/H315A with NADPH on first despite the higher NADPH $K_m$.

## ■ REFERENCES


(1) Parsons, D. W., Jones, S., Zhang, X., Lin, J. C., Leary, R. J., Angenendt, P., Mankoo, P., Carter, H., Siu, I. M., Gallia, G. L., Olivi, A., McLendon, R., Rasheed, B. A., Keir, S., Nikolskaya, T., Nikolsky, Y., Busam, D. A., Tekleab, H., Diaz, L. A., Jr., Hartigan, J., Smith, D. R., Strausberg, R. L., Marie, S. K., Shinjo, S. M., Yan, H., Riggins, G. J., Bigner, D. D., Karchin, R., Papadopoulos, N., Parmigiani, G., Vogelstein, B., Velculescu, V. E., and Kinzler, K. W. (2008) An integrated genomic analysis of human glioblastoma multiforme. *Science 321*, 1807−1812.

(2) Mardis, E. R., Ding, L., Dooling, D. J., Larson, D. E., McLellan, M. D., Chen, K., Koboldt, D. C., Fulton, R. S., Delehaunty, K. D., McGrath, S. D., Fulton, L. A., Locke, D. P., Magrini, V. J., Abbott, R. M., Vickery, T. L., Reed, J. S., Robinson, J. S., Wylie, T., Smith, S. M., Carmichael, L., Eldred, J. M., Harris, C. C., Walker, J., Peck, J. B., Du, F., Dukes, A. F., Sanderson, G. E., Brummett, A. M., Clark, E., McMichael, J. F., Meyer, R. J., Schindler, J. K., Pohl, C. S., Wallis, J. W., Shi, X., Lin, L., Schmidt, H., Tang, Y., Haipek, C., Wiechert, M. E., Ivy, J. V., Kalicki, J., Elliott, G., Ries, R. E., Payton, J. E., Westervelt, P., Tomasson, M. H., Watson, M. A., Baty, J., Heath, S., Shannon, W. D., Nagarajan, R., Link, D. C., Walter, M. J., Graubert, T. A., DiPersio, J. F., Wilson, R. K., and Ley, T. J. (2009) Recurring mutations found by sequencing an acute myeloid leukemia genome. *N. Engl. J. Med. 361*, 1058−1066.

(3) Green, A., and Beer, P. (2010) Somatic mutations of IDH1 and IDH2 in the leukemic transformation of myeloproliferative neoplasms. *N. Engl. J. Med. 362*, 369−370.

(4) Gross, S., Cairns, R. A., Minden, M. D., Driggers, E. M., Bittinger, M. A., Jang, H. G., Sasaki, M., Jin, S., Schenkein, D. P., Su, S. M., Dang, L., Fantin, V. R., and Mak, T. W. (2010) Cancer-associated metabolite 2-hydroxyglutarate accumulates in acute myelogenous leukemia with isocitrate dehydrogenase 1 and 2 mutations. *J. Exp. Med. 207*, 339−344.

(5) Zhang, Y., Wei, H., Tang, K., Lin, D., Zhang, C., Mi, Y., Wang, L., Wang, C., Wang, M., and Wang, J. (2012) Mutation analysis of isocitrate dehydrogenase in acute lymphoblastic leukemia. *Genet. Test. Mol. Biomarkers 16*, 991−995.

(6) Patnaik, M. M., Hanson, C. A., Hodnefield, J. M., Lasho, T. L., Finke, C. M., Knudson, R. A., Ketterling, R. P., Pardanani, A., and Tefferi, A. (2012) Differential prognostic effect of IDH1 versus IDH2 mutations in myelodysplastic syndromes: A Mayo Clinic study of 277 patients. *Leukemia 26*, 101−105.

(7) Amary, M. F., Bacsi, K., Maggiani, F., Damato, S., Halai, D., Berisha, F., Pollock, R., O'Donnell, P., Grigoriadis, A., Diss, T., Eskandarpour, M., Presneau, N., Hogendoorn, P. C., Futreal, A., Tirabosco, R., and Flanagan, A. M. (2011) IDH1 and IDH2 mutations are frequent events in central chondrosarcoma and central and periosteal chondromas but not in other mesenchymal tumours. *J. Pathol. 224*, 334−343.

(8) Cairns, R. A., Iqbal, J., Lemonnier, F., Kucuk, C., de Leval, L., Jais, J. P., Parrens, M., Martin, A., Xerri, L., Brousset, P., Chan, L. C., Chan, W. C., Gaulard, P., and Mak, T. W. (2012) IDH2 mutations are frequent in angioimmunoblastic T-cell lymphoma. *Blood 119*, 1901−1903.

(9) Borger, D. R., Tanabe, K. K., Fan, K. C., Lopez, H. U., Fantin, V. R., Straley, K. S., Schenkein, D. P., Hezel, A. F., Ancukiewicz, M., Liebman, H. M., Kwak, E. L., Clark, J. W., Ryan, D. P., Deshpande, V., Dias-Santagata, D., Ellisen, L. W., Zhu, A. X., and Iafrate, A. J. (2012) Frequent mutation of isocitrate dehydrogenase (IDH)1 and IDH2 in cholangiocarcinoma identified through broad-based tumor genotyping. *Oncologist 17*, 72−79.

(10) Ghiam, A. F., Cairns, R. A., Thoms, J., Dal Pra, A., Ahmed, O., Meng, A., Mak, T. W., and Bristow, R. G. (2012) IDH mutation status in prostate cancer. *Oncogene 31*, 3826.

(11) Soundar, S., Danek, B. L., and Colman, R. F. (2000) Identification by mutagenesis of arginines in the substrate binding site of the porcine NADP-dependent isocitrate dehydrogenase. *J. Biol. Chem. 275*, 5606−5612.

(12) Jennings, G. T., Minard, K. I., and McAlister-Henn, L. (1997) Expression and mutagenesis of mammalian cytosolic $NADP^+$-specific isocitrate dehydrogenase. *Biochemistry 36*, 13743−13747.

(13) Yan, H., Parsons, D. W., Jin, G., McLendon, R., Rasheed, B. A., Yuan, W., Kos, I., Batinic-Haberle, I., Jones, S., Riggins, G. J., Friedman, H., Friedman, A., Reardon, D., Herndon, J., Kinzler, K. W., Velculescu, V. E., Vogelstein, B., and Bigner, D. D. (2009) IDH1 and IDH2 mutations in gliomas. *N. Engl. J. Med. 360*, 765−773.

(14) Leonardi, R., Subramanian, C., Jackowski, S., and Rock, C. O. (2012) Cancer-associated isocitrate dehydrogenase mutations inactivate NADPH-dependent reductive carboxylation. *J. Biol. Chem. 287*, 14615−14620.

(15) Dang, L., White, D. W., Gross, S., Bennett, B. D., Bittinger, M. A., Driggers, E. M., Fantin, V. R., Jang, H. G., Jin, S., Keenan, M. C., Marks, K. M., Prins, R. M., Ward, P. S., Yen, K. E., Liau, L. M., Rabinowitz, J. D., Cantley, L. C., Thompson, C. B., Vander Heiden, M. G., and Su, S. M. (2009) Cancer-associated IDH1 mutations produce 2-hydroxyglutarate. *Nature 462*, 739−744.

(16) Xu, W., Yang, H., Liu, Y., Yang, Y., Wang, P., Kim, S. H., Ito, S., Yang, C., Xiao, M. T., Liu, L. X., Jiang, W. Q., Liu, J., Zhang, J. Y., Wang, B., Frye, S., Zhang, Y., Xu, Y. H., Lei, Q. Y., Guan, K. L., Zhao, S. M., and Xiong, Y. (2011) Oncometabolite 2-hydroxyglutarate is a

competitive inhibitor of α-ketoglutarate-dependent dioxygenases. *Cancer Cell 19*, 17−30.
(17) Figueroa, M. E., Abdel-Wahab, O., Lu, C., Ward, P. S., Patel, J., Shih, A., Li, Y., Bhagwat, N., Vasanthakumar, A., Fernandez, H. F., Tallman, M. S., Sun, Z., Wolniak, K., Peeters, J. K., Liu, W., Choe, S. E., Fantin, V. R., Paietta, E., Lowenberg, B., Licht, J. D., Godley, L. A., Delwel, R., Valk, P. J., Thompson, C. B., Levine, R. L., and Melnick, A. (2010) Leukemic IDH1 and IDH2 mutations result in a hypermethylation phenotype, disrupt TET2 function, and impair hematopoietic differentiation. *Cancer Cell 18*, 553−567.
(18) Lu, C., Ward, P. S., Kapoor, G. S., Rohle, D., Turcan, S., Abdel-Wahab, O., Edwards, C. R., Khanin, R., Figueroa, M. E., Melnick, A., Wellen, K. E., O'Rourke, D. M., Berger, S. L., Chan, T. A., Levine, R. L., Mellinghoff, I. K., and Thompson, C. B. (2012) IDH mutation impairs histone demethylation and results in a block to cell differentiation. *Nature 483*, 474−478.
(19) Turcan, S., Rohle, D., Goenka, A., Walsh, L. A., Fang, F., Yilmaz, E., Campos, C., Fabius, A. W., Lu, C., Ward, P. S., Thompson, C. B., Kaufman, A., Guryanova, O., Levine, R., Heguy, A., Viale, A., Morris, L. G., Huse, J. T., Mellinghoff, I. K., and Chan, T. A. (2012) IDH1 mutation is sufficient to establish the glioma hypermethylator phenotype. *Nature 483*, 479−483.
(20) Pollock, V. V., and Barber, M. J. (2001) Kinetic and mechanistic properties of biotin sulfoxide reductase. *Biochemistry 40*, 1430−1440.
(21) Otwinowski, Z., and Minor, W. (1997) Processing of X-ray diffraction data collected in oscillation mode. *Methods Enzymol. 276*, 307−326.
(22) McCoy, A. J., Grosse-Kunstleve, R. W., Adams, P. D., Winn, M. D., Storoni, L. C., and Read, R. J. (2007) Phaser crystallographic software. *J. Appl. Crystallogr. 40*, 658−674.
(23) Collaborative Computational Project, Number 4 (1994) The CCP4 suite: Programs for protein crystallography. *Acta Crystallogr. D50*, 760−763.
(24) Murshudov, G. N., Vagin, A. A., and Dodson, E. J. (1997) Refinement of macromolecular structures by the maximum-likelihood method. *Acta Crystallogr. D53*, 240−255.
(25) Chen, V. B., Arendall, W. B., Headd, J. J., Keedy, D. A., Immormino, R. M., Kapral, G. J., Murray, L. W., Richardson, J. S., and Richardson, D. C. (2010) MolProbity: All-atom structure validation for macromolecular crystallography. *Acta Crystallogr. D66*, 12−21.
(26) Emsley, P., and Cowtan, K. (2004) Coot: Model-building tools for molecular graphics. *Acta Crystallogr. D60*, 2126−2132.
(27) *Molecular Operating Environment (MOE)*, version 2011.10 (2011) Chemical Computing Group Inc., Montreal.
(28) Miranker, A., and Karplus, M. (1991) Functionality maps of binding sites: A multiple copy simultaneous search method. *Proteins 11*, 29−34.
(29) Aktas, D. F., and Cook, P. F. (2009) A lysine-tyrosine pair carries out acid-base chemistry in the metal ion-dependent pyridine dinucleotide-linked β-hydroxyacid oxidative decarboxylases. *Biochemistry 48*, 3565−3577.
(30) Yang, B., Zhong, C., Peng, Y., Lai, Z., and Ding, J. (2010) Molecular mechanisms of "off-on switch" of activities of human IDH1 by tumor-associated mutation R132H. *Cell Res. 20*, 1188−1200.
(31) Bleeker, F. E., Lamba, S., Leenstra, S., Troost, D., Hulsebos, T., Vandertop, W. P., Frattini, M., Molinari, F., Knowles, M., Cerrato, A., Rodolfo, M., Scarpa, A., Felicioni, L., Buttitta, F., Malatesta, S., Marchetti, A., and Bardelli, A. (2009) IDH1 mutations at residue p.R132 (IDH1(R132)) occur frequently in high-grade gliomas but not in other solid tumors. *Hum. Mutat. 30*, 7−11.
(32) Ward, P. S., Cross, J. R., Lu, C., Weigert, O., Abel-Wahab, O., Levine, R. L., Weinstock, D. M., Sharp, K. A., and Thompson, C. B. (2012) Identification of additional IDH mutations associated with oncometabolite R(−)-2-hydroxyglutarate production. *Oncogene 31*, 2491−2498.
(33) Xu, X., Zhao, J., Xu, Z., Peng, B., Huang, Q., Arnold, E., and Ding, J. (2004) Structures of human cytosolic NADP-dependent isocitrate dehydrogenase reveal a novel self-regulatory mechanism of activity. *J. Biol. Chem. 279*, 33946−33957.
(34) Pietrak, B., Zhao, H., Qi, H., Quinn, C., Gao, E., Boyer, J. G., Concha, N., Brown, K., Duraiswami, C., Wooster, R., Sweitzer, S., and Schwartz, B. (2011) A tale of two subunits: How the neomorphic R132H IDH1 mutation enhances production of αHG. *Biochemistry 50*, 4804−4812.
(35) Plaut, G. W., and Aogaichi, T. (1968) Purification and properties of diphosphopyridine nuleotide-linked isocitrate dehydrogenase of mammalian liver. *J. Biol. Chem. 243*, 5572−5583.
(36) Mullen, A. R., Wheaton, W. W., Jin, E. S., Chen, P. H., Sullivan, L. B., Cheng, T., Yang, Y., Linehan, W. M., Chandel, N. S., and DeBerardinis, R. J. (2011) Reductive carboxylation supports growth in tumour cells with defective mitochondria. *Nature 481*, 385−388.
(37) Filipp, F. V., Scott, D. A., Ronai, Z. A., Osterman, A. L., and Smith, J. W. (2012) Reverse TCA cycle flux through isocitrate dehydrogenases 1 and 2 is required for lipogenesis in hypoxic melanoma cells. *Pigm. Cell Melanoma Res. 25*, 375−383.
(38) Wise, D. R., Ward, P. S., Shay, J. E., Cross, J. R., Gruber, J. J., Sachdeva, U. M., Platt, J. M., DeMatteo, R. G., Simon, M. C., and Thompson, C. B. (2011) Hypoxia promotes isocitrate dehydrogenase-dependent carboxylation of α-ketoglutarate to citrate to support cell growth and viability. *Proc. Natl. Acad. Sci. U.S.A. 108*, 19611−19616.
(39) Siebert, G., Carsiotis, M., and Plaut, G. W. (1957) The enzymatic properties of isocitric dehydrogenase. *J. Biol. Chem. 226*, 977−991.
(40) Cotelesage, J. J., Puttick, J., Goldie, H., Rajabi, B., Novakovski, B., and Delbaere, L. T. (2007) How does an enzyme recognize $CO_2$? *Int. J. Biochem. Cell Biol. 39*, 1204−1210.
(41) Burton, R. L., Hanes, J. W., and Grant, G. A. (2008) A stopped flow transient kinetic analysis of substrate binding and catalysis in *Escherichia coli* D-3-phosphoglycerate dehydrogenase. *J. Biol. Chem. 283*, 29706−29714.
(42) Northrop, D. B., and Cleland, W. W. (1974) The kinetics of pig heart triphosphopyridine nucleotide-isocitrate dehydrogenase. II. Dead-end and multiple inhibition studies. *J. Biol. Chem. 249*, 2928−2931.
(43) Uhr, M. L., Thompson, V. W., and Cleland, W. W. (1974) The kinetics of pig heart triphosphopyridine nucleotide-isocitrate dehydrogenase. I. Initial velocity, substrate and product inhibition, and isotope exchange studies. *J. Biol. Chem. 249*, 2920−2927.
(44) Segel, I. H. (1975) *Enzyme Kinetics: Behavior and Analysis of Rapid Equilibrium and Steady-State Enzyme Systems*, Wiley, New York.
(45) Cook, P. F., and Cleland, W. W. (1981) Mechanistic deductions from isotope effects in multireactant enzyme mechanisms. *Biochemistry 20*, 1790−1796.
(46) Cook, P. F. (1981) Kinetic and regulatory mechanisms of enzymes from isotope effects. In *Enzyme Mechanisms from Isotope Effects* (Cook, P. F., Ed.) pp 203−228, CRC Press, Boca Raton, FL.
(47) O'Leary, M. H., and Limburg, J. A. (1977) Isotope effect studies of the role of metal ions in isocitrate dehydrogenase. *Biochemistry 16*, 1129−1135.
(48) Grissom, C. B., and Cleland, W. W. (1988) Isotope effect studies of the chemical mechanism of pig heart NADP isocitrate dehydrogenase. *Biochemistry 27*, 2934−2943.
(49) Ricci, G., Turella, P., De Maria, F., Antonini, G., Nardocci, L., Board, P. G., Parker, M. W., Carbonelli, M. G., Federici, G., and Caccuri, A. M. (2004) Binding and kinetic mechanisms of the zeta class glutathione transferase. *J. Biol. Chem. 279*, 33336−33342.
(50) Neckles, C., Shah, S., Pan, P., Bommineni, G., Hirschbeck, M. W., Yu, W., Liu, N., Kisker, C., and Tonge, P. J. (2013) Single Nucleotide Polymorphism Changes Substrate Binding Mechanism and Inhibitor Specificity of *Yersinia pestis* Enoyl-ACP Reductase FabV. 23rd Enzyme Mechanism Conference, Coronado, CA.